RF Project 3329
Report   4

THE OHIO STATE UNIVERSITY

RESEARCH FOUNDATION

1314 KINNEAR ROAD   COLUMBUS, OHIO   43212

EFFECTS OF WEIGHTLESSNESS ON THE DEVELOPMENT OF THE

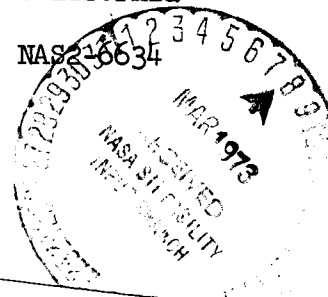VESTIBULAR APPARATUS AND OCULAR NYSTAGMUS IN THE RAT

Dr. David L. Clark

Department of Anatomy

1 October 1971 - 30 September 1972

NASA, AMES RESEARCH CENTER
Moffett Field, California

Contract No. NAS2-6634

ANNUAL

REPORT

By

THE OHIO STATE UNIVERSITY
RESEARCH FOUNDATION

1314 KINNEAR RD.
COLUMBUS, OHIO 43212

On................ EFFECTS OF WEIGHTLESSNESS ON THE DEVELOPMENT

.... OF THE VESTIBULAR APPARATUS AND OCULAR

.... NYSTAGMUS IN THE RAT

Submitted by.......Dr. David L. Clark................

.... Department of Anatomy

i

TABLE OF CONTENTS

LIST OF FIGURES

LIST OF TABLES

PART I

CONSTRUCTION OF THE CHRONIC 2G CENTRIFUGE

In formulating design characteristics of the Chronic 2g Centrifuge, several constraints were considered in order to ensure the constancy and reliability of vestibular data retrieved from the rats housed on board the centrifuge. A prime concern was that of reliability. The data would have little meaning if the unit were inoperable for any amount of time, requiring repair or maintenance. It was predetermined that any maintenance required should be scheduled maintenance which could be administered at intervals of at least several months. The centrifuge must also run continuously and at a constant velocity. The centrifuge was to have as large a radius arm as possible in order to minimize the coriolis phenomena effects that could alter vestibular system response. Both the velocity and radius, however, were to be infinitely variable, within certain specified limits, in order to provide flexibility in experimental design if the need arose at a future date. The centrifuge was to provide living space for a minimum of 20 rats, which were to be housed in standard 18" x 10" x 7" deep laboratory cages. The rats were to receive food and water ad libitum. It was emphasized that wobble and vibration be kept to a minimum. The cages were to be oriented on the radius arm such that at any speed, from zero to maximum velocity, the floor of the cage was to be perpendicular to the resultant gravity vector.

The Electrical Shop in the Department of Electrical Engineering at The Ohio State University agreed to design and construct the centrifuge. They agreed to a six-month deadline but requested that the design stage be kept to a minimum in order to assure completion with the six-month period. This request proved to be an asset in speeding construction and completion of the centrifuge within the allotted time span.

The dimensions of the centrifuge were dictated by the size of the room in which it was to be housed. It was decided that the maximum radius was to be 10.5 ft. By dividing the length of the circumference by the length of each cage, it was determined that we could easily accommodate 20 cages at the maximum radius. At shorter radii fewer cages can be accommodated at any one particular radius because of the reduced circumference. We have the option, however, of staggering cages at several different radii. This will be available in later experiments in which we wish to expose different populations of experimental animals to different g levels while maintaining a constant velocity of rotation and coriolis phenomena. The design includes the potential of positioning a single cage or a vertical stack of several cages over the center axis of the centrifuge, thus positioning the rats at essentially zero radius, 1g. However, since they will turn at the same velocity as the rest of the centrifuge they will be exposed to the identical potential coriolis phenomena.

1

The standard polyethylene laboratory cages are individually held in an aluminum cage holder. The cage holder is formed and heliarc welded on a jig (Fig. 1). The individual cage slips into the cage holder (Fig. 2) and can be easily removed for cage cleaning. This size cage can accommodate up to four adult rats or one rat with a litter.

A gimbal cage support suspension device was accepted following tests on a prototype (Fig. 2). The gimbal consists of a ball and socket joint and a horizontal axis (Fig. 3). The ball is made of brass and can rotate sufficiently within the socket assembly to maintain alignment of the horizontal axis. The cage holder is suspended from the ball and socket by a short support stud riveted by means of a flange to the cage support bracket (Fig. 3). The stud slips through a hole in the brass ball and the assembly is secured by a circlip at the end of the stud. This gimbal has proved to present a minimum of friction and is satisfactory in maintaining the floor of the cage perpendicular to the gravity vector, regardless of speed of rotation (Fig. 4).

Food and water are provided for the rats by a conventional pellet tray and water bottle holder incorporated into the cage lid. Inadvertent water loss from the water bottle has not proved to be a problem. This may be partially due to the fact that we have selected dropper spouts with a relatively small diameter opening and have cut the spout shaft to keep it as short as possible and still allow the rat easy access to the water.

Each cage support is anchored to its pair of radius arms or radius arm extensions by means of two pinch clamps, one directly below each gimbal. The clamp is secured by tightening a single bolt. The clamp holds the cage support in its position by friction and the system is designed so that the cage may be positioned at any radius from the hub to the outer limit of the radius arm extensions. The clamps are aligned on the box channels making up the radius arms and radius arm extensions so that if both cage clamps should fail, which is unlikely, the cage would slide to the maximum radius of the radius arms or radius extension arms. They would not lose their attachment to the centrifuge and thus could not fly off the centrifuge producing a potential hazard to personnel.

The simplest and most rigid radius arm construction was employed. Box aluminum alloy channel (2" x 4") was chosen for radius arms and radius arm extensions. This construction gives the greatest rigidity and strength per pound weight and, at the same time, simplifies the method of assembly. At critical points such as the point at which each radius arm is joined to the hub and where the extension arm is attached, a sleeve fit was used for strength and ease of assembly. The internal and external sections of each sleeve were then secured with bolts (Fig. 5).

Each radius arm assembly was divided into two parts. The inner is the radius arm proper and the outer is the radius arm extension. This method was devised for ease of construction and also to provide more

2
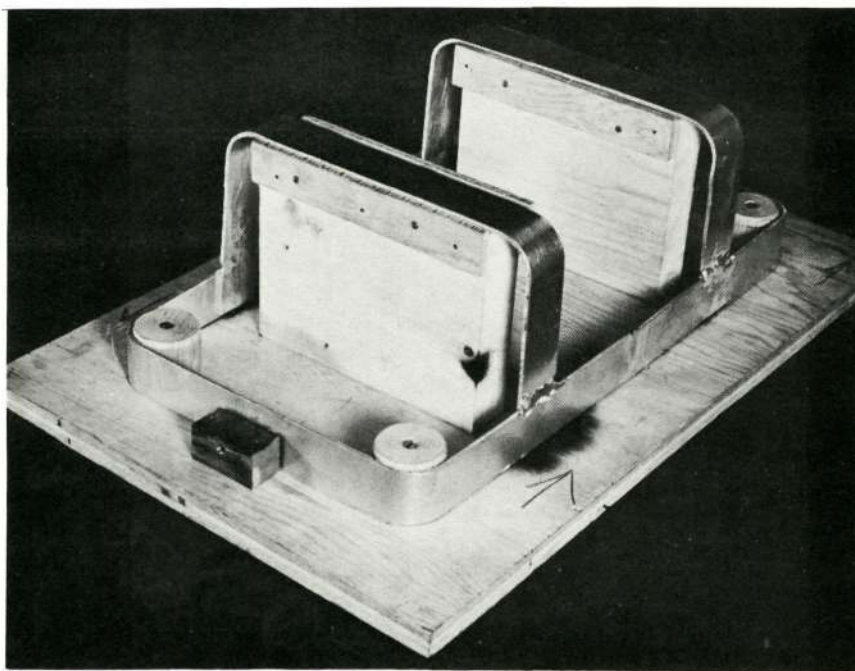
Fig. 1 - Jig developed to form and weld aluminum cage holder
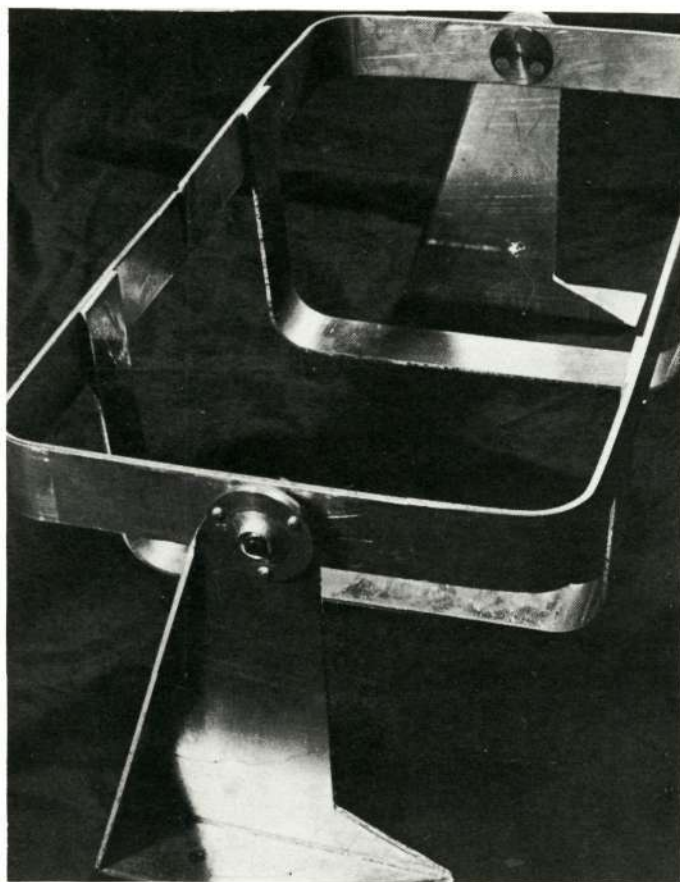
Fig. 2 - Cage holder for standard laboratory cage measuring 18" x 10" x 7" deep
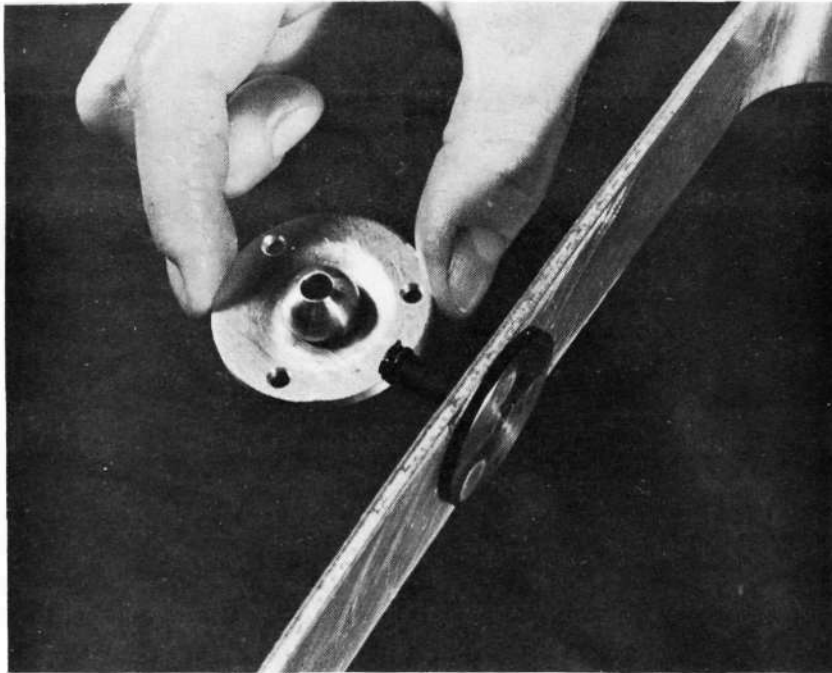
Fig. 3 - Detail of gimbal unit, with brass ball and
support stud, which allows swivel of cage
holder on centrifuge
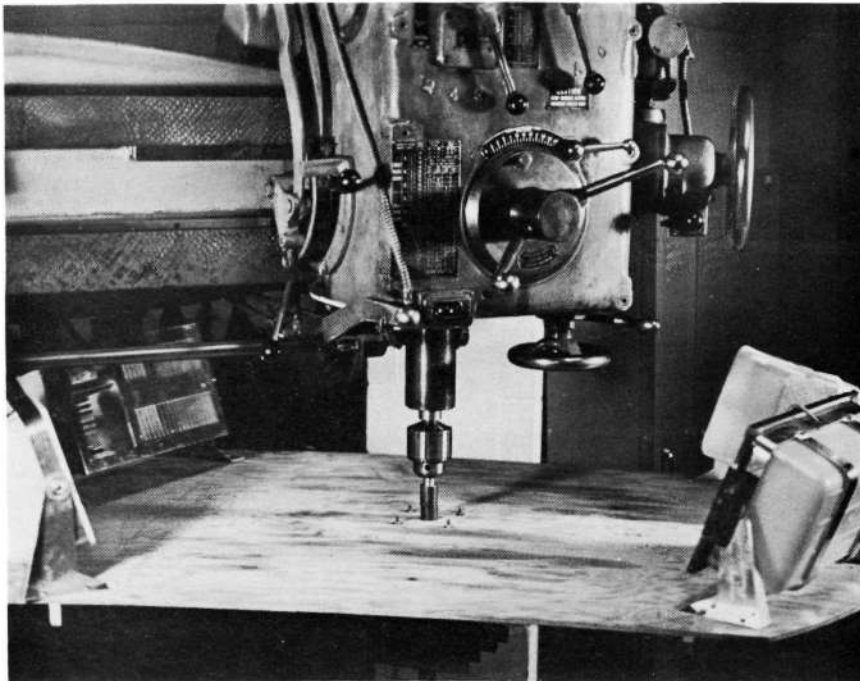
Fig. 4 - Cages on test device rotating at about 100 rpm
(Note cage tilt in response to combined gravi-
tational and centrifugal forces)

4
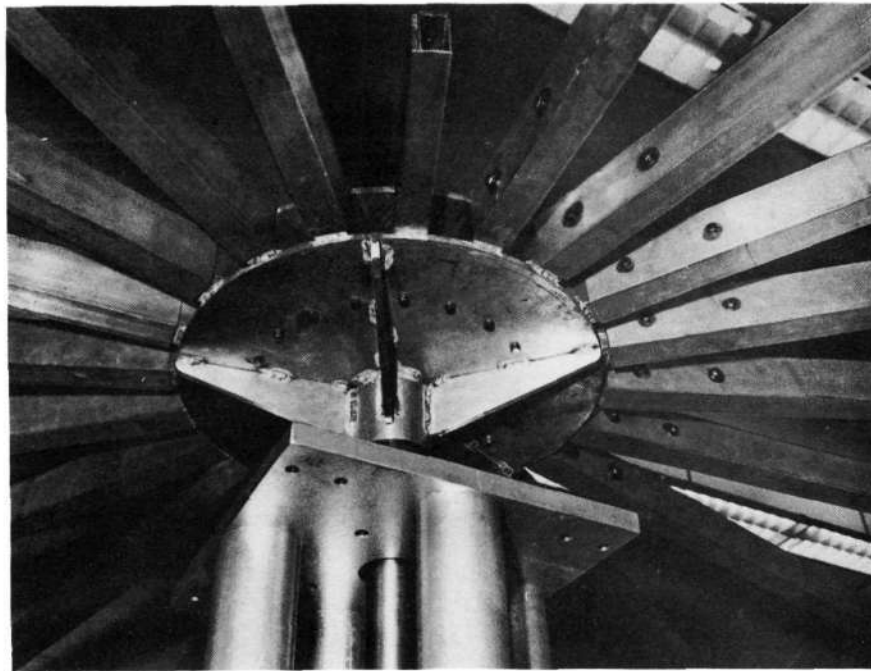
Fig. 5 - Radius arms are mated to hub assembly by sleeve
fit over stud and secured by bolts

Fig. 6 - Hub with radius arms attached
(Maximum radius is 5.25 ft)

5

flexibility in the operation of the centrifuge. With just the radius arms secured to the hub, the maximum effective radius of the centrifuge is 5.25 ft (Fig. 6). This considerably reduces the weight of the centrifuge wheel and also reduces wind-loading. The power requirements for driving this effectively smaller centrifuge are reduced and thus, with the power unit available, higher rotational velocities can be achieved. The increase in rotational velocity could produce higher g levels or higher potential coriolis stimulation or both, on the experimental design.

The radius arm extension is a "Y" shaped extension arm. The base of the "Y" plugs into the terminal end of the radius arm and extends the radius of the centrifuge to 10.5 ft (Fig. 7). The use of the radius arm extension increases the total weight and wind-loading force of the centrifuge wheel. The increased radius, however, reduces the potential coriolis effect generated at any particular g level produced. This has proved to be an important stimulus parameter when the vestibular system is being examined.

The hub assembly is the critical part of the centrifuge. It is required to anchor the radius arms, transmit torque from the vertical shaft to the radius arms, and transmit the entire weight of the super-structure to the vertical drive shaft and its support bearing. In order to ensure success of the hub assembly construction a careful design was completed and a wooden mock-up was built (Figs. 8 and 9). It was decided that the hub be constructed as a single welded unit in order to provide strength. The same aluminum alloy was used in order to help reduce weight. The hub assembly is constructed of two 0.5-inch-thick plates 22 inches in diameter. They fit around a 4-inch outside diameter center sleeve 13.5 inches long. A steel quick-disconnect pulley hub fits into each end of the sleeve. These pulley hubs are keyed for a two-inch shaft. The circular plates are strengthened by five triangular gussets welded between the plate and center sleeve on both the upper and lower side of the assembly (Fig. 10).

Twenty specially welded and machined box studs were incorporated into the hub assembly between the circular disks. Each stud is 15 inches long and is individually fitted to accept its corresponding radius arm, with a minimum of clearance (Fig. 10). The individual components of the hub are heliarc welded to form an integral assembly.

The base is made of four-inch steel channel welded into a six-foot square box frame (Fig. 11). Two parallel cross braces directly support the load and transfer it to the box frame directly and also by means of four cross angle braces. In order to achieve added support and stability, each side of the box frame is provided with a bolt-on leg that adds ten feet to the support base in each direction (Fig. 12).

The pedestal assembly incorporates the drive motor, speed reducer, drive shaft, and support bearings (Fig. 13). Four hollow steel cylinders,
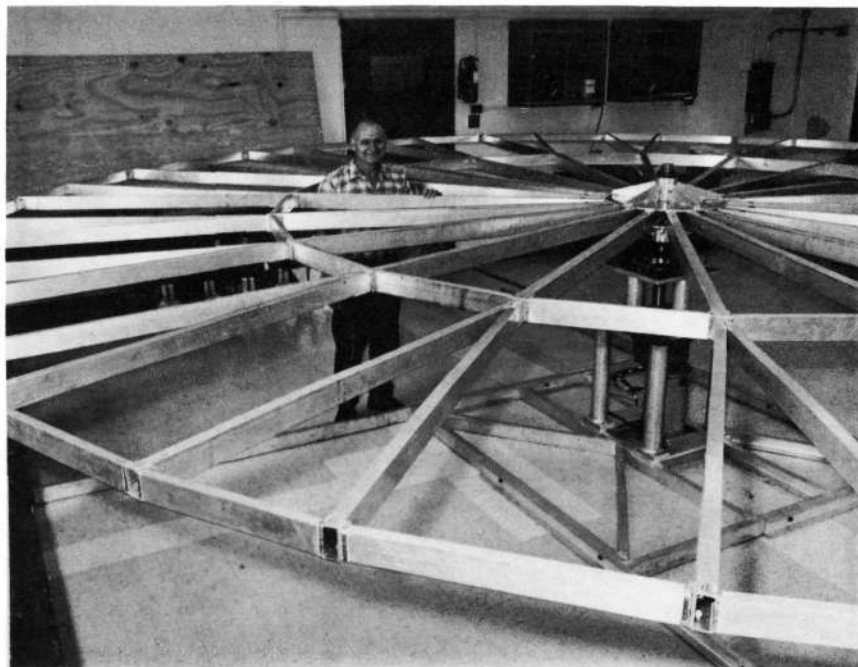
Fig. 7 - Radius extensions mated to radius arms
(Maximum radius is 10.5 ft)
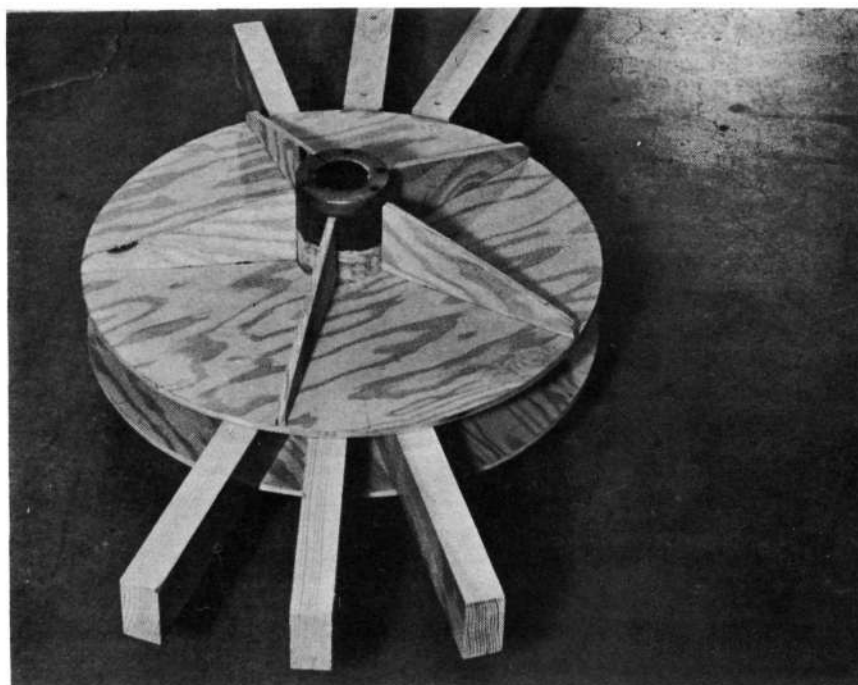
Fig. 8 - Wooden mock-up of centrifuge hub with top
support disk and gussets in place
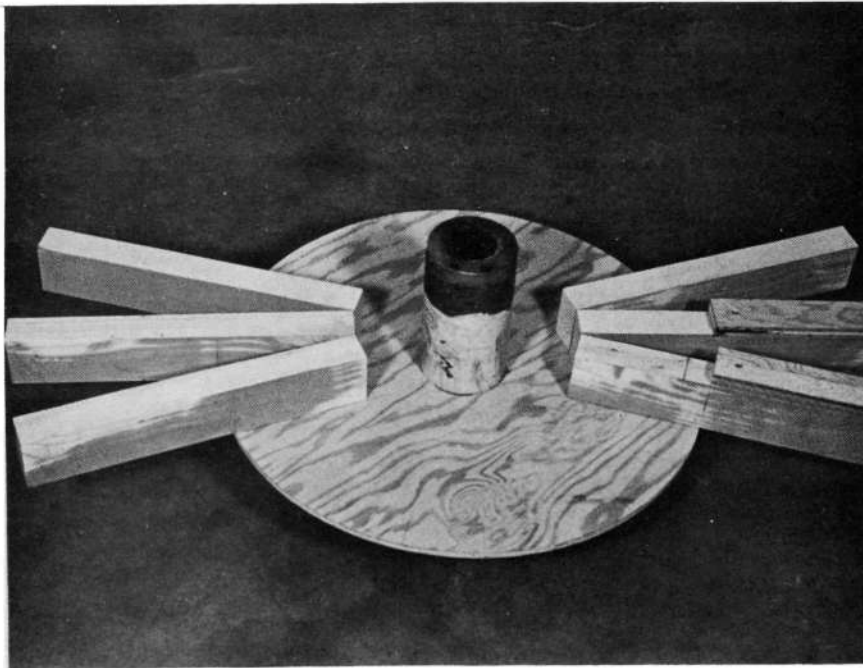
Fig. 9 - Wooden mock-up of centrifuge hub with top
support disk removed revealing position of
studs
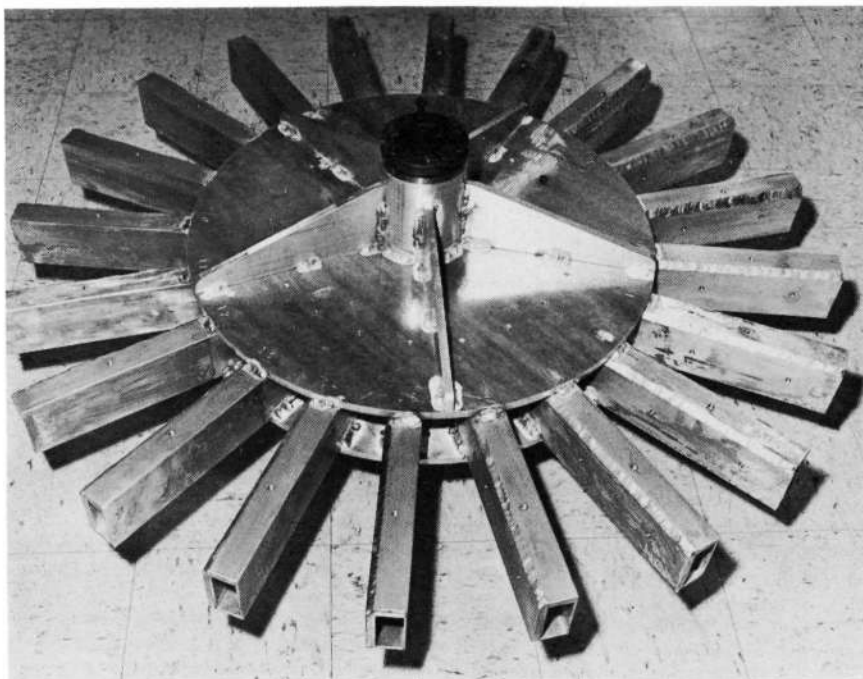
Fig. 10 - Completed hub assembly welded into a single
unit ready for assembly
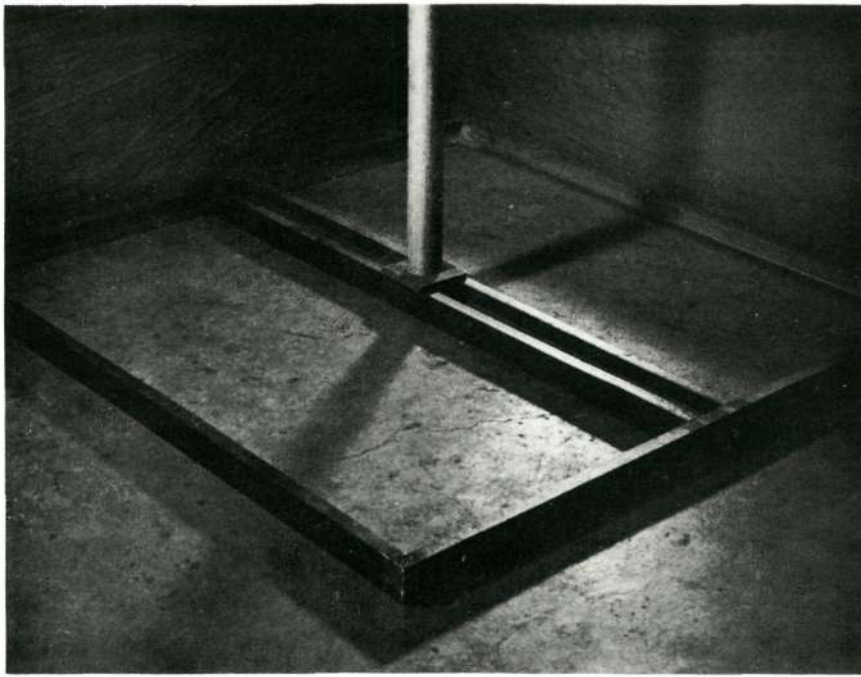
Fig. 11 - Six-foot square centrifuge support base
(Center post represents axis of centrifuge)
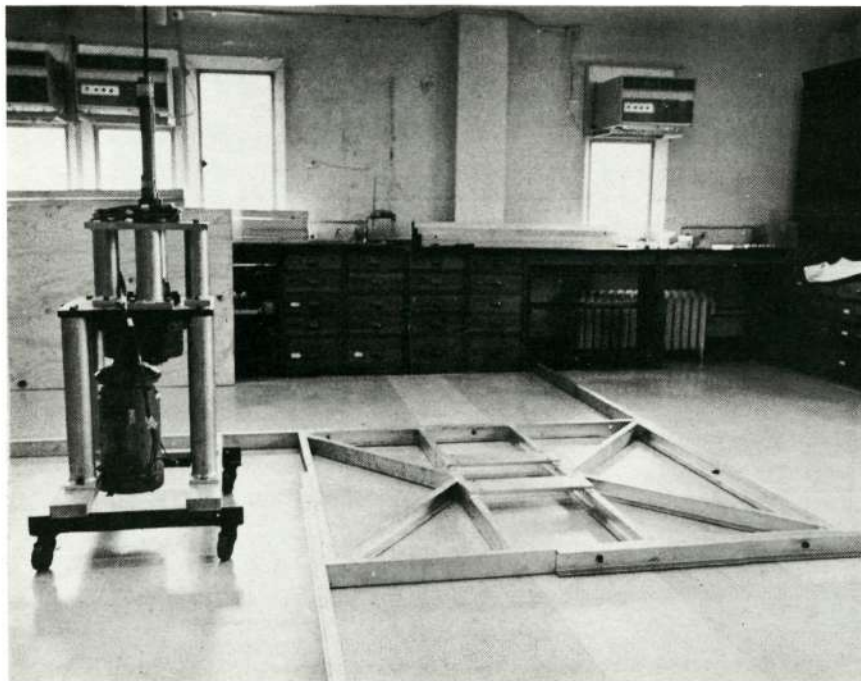
Fig. 12 - Six-foot square centrifuge support base with
cross braces and bolt-on legs
(At left is pedestal assembly)

9

Fig. 13 - Pedestal assembly with drive motor, speed reducer, support bearings, and drive shaft
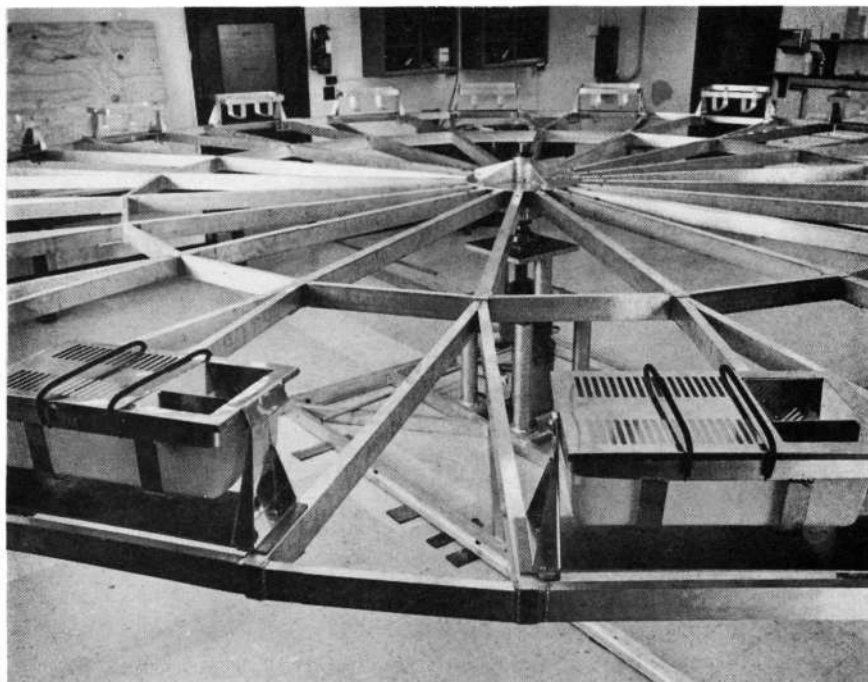
Fig. 14 - Completed centrifuge with cages holders and cages positioned at maximum radius

measuring 3.5 x 22.5 inches, support the base plates of the pedestal assembly. Four hollow steel cylinders, 3.5 x 9.5 inches, are bolted to the base plate and support the upper plate of the pedestal assembly. The steel base plate is 20 x 20 x 1 inch thick and is machined on the upper and lower surfaces to provide a smooth flat surface. The steel upper plate is 16 x 16 x 1 inch thick.

The centrifuge wheel weight and maximum diameter were taken into consideration in estimating the power required to drive the centrifuge. It was found that the leading edge of all cages as they rotated displaced a considerable quantity of air, thus developing a wind-loading force opposing the rotation of the centrifuge. Several tests were attempted to determine a value for this force, and a rough estimate was determined. In addition, it was found that the wind-loading effect on the leading edge of the combined radius arms also contributed to this force. Based on these estimates it was concluded that a three-horsepower direct current motor would be adequate to drive the centrifuge within the speed ranges necessary to generate at least 2g at any point along the radius arm of the centrifuge.

The drive motor selected is a General Electric, Type L186ATC, three-horsepower direct current motor. It is suspended in a vertical position in the base of the pedestal. It is coupled directly to a Boston Gear Optimount 17:1 flanged speed reducer. The speed reducer is bolted to the underside of the base plate and accepts the 2 7/16-inch keyed drive shaft. The drive shaft reduces to a two-inch diameter above the bearing supports. The maximum motor speed is 1750 rpm. The speed reducer allows the output drive shaft to turn at a maximum of about 100 rpm. Tests of the completed centrifuge have shown that maximum speed can be approximated with the radius arm and inner ring assembled (Fig. 14). With the radius arm extensions added, the maximum speed is approximately 30 rpm. The only maintenance required is to change the speed reducer oil once every 40 days, and to periodically inspect and replace the motor brushes.

Centrifuge speed is controlled by a Boston Gear Ratiotrol, produced by the Boston Gear Division of North American Rockwell. This device is a full-wave, solid-state SCR control and utilizes modular construction and transistorized circuitry, including integrated circuits. The control will accelerate the centrifuge from zero to a present velocity. It will maintain this speed continuously within ±1% of motor base speed.

PART II

INTRODUCTION

The vestibular system of equilibrium includes both afferent and efferent components. The sensory end organ is made up of two functional subunits. One of these is sensitive to gravity and linear acceleration and the second of these is sensitive to turning movements of the head, viz., angular acceleration. Linear acceleration is detected by the macula of the utriculus and possibly the macula of the sacculus. Angular acceleration is detected by the cristae ampullares of the three semicircular canals. The vestibular end organ provides the central nervous system with information as to the position of the head with respect to gravity and the acceleration of the head in space. The efferent components of this system are related to antigravity musculature, muscles associated with movements of the head and neck, and extraocular muscles. In addition, the vestibular system has been associated with the autonomic nervous system and arousal.

Two other sensory systems also play a role in maintenance of equilibrium. First, the visual system functions primarily to maintain a visual horizon. Second, the proprioceptive system provides information as to the position of the head with respect to the body, the position of limbs with respect to the body, and the position of the limbs with respect to the substratusm. All three of these systems function together in order to assess the position of the head in space, the position of the head with respect to the body, and the position of the limbs relative to the body and the substratusm.

The exact role played by each of these systems, or by the individual parts of each system, is not yet clearly known. In this study an attempt was made to establish a quantitative measurement of the ability of the white rat to utilize these equilibrium systems in order to maintain his balance during a dynamic situation.

MATERIALS AND METHODS

Two groups of rats were utilized. One group, the 1g controls, were adult rats that had been raised under standard laboratory conditions under the effects of the earth standard gravity of 1g. The second group, the 2g experimentals, were adult rats that had been maintained on a centrifuge for a minimum of 60 days, 24 hours per day.

The centrifuge was a small table top device measuring about 1 m in diameter. In order to produce the required 2g environment, the centrifuge was rotated at 60 rpm. The cages were tilted inward about 30° in order to position the 2g gravity vector perpendicular to the floor of the cage. Both groups of rats received food and water ad libidum.

The device used to test the dynamic equilibrium characteristics of the rats was designed after the rail device for monkeys, described by Igarashi (1968). The rat rail device measures 3 ft. long, 1½ ft. wide and 2 ft. high. Extending beyond the test box are two start boxes, one located at each end. Each is separated from the test box by a sliding door. A rail, 1 inch in diameter, runs the length of the box and is cross-shaped in cross-section. The floor of the start boxes and the test box is an electric shock grid. The rail is at the same level as the floor of the start boxes, and is 4 inches above the electrified grid floor of the test box. The rail is connected to a D.C. motor and the rate of rotation of the rail can be controlled from 0-25 rpm.

PROCEDURE

During a single testing session, a rat was placed in the start box for 15 seconds at one end of the rail. The sliding door was raised and a light turned on at the opposite end of the test box. After five seconds the grid in the start box was electrified. The rat was allowed to remain in the test box for up to 60 seconds. There were ten 1g control and ten 2g experimental rats. Each rat was tested first in the stationary rail test; i.e., each animal was run for ten trials each day for ten consecutive days. Following the stationary rail test, each rat was then tested in the rotating rail test. Each animal was run for one trial at each of the following rail rotation speeds: 0, 5, 10, 15, 20, and 25 rpm. The procedure for the rotating rail test was continued for three consecutive days. All 2g rats were returned to the 2g centrifuge following completion of tests each day. All testing was done at 1g.

Three sets of data were collected from each group of animals for each trial. First, it was determined if the rat actively avoided the shock in the start box that was initiated five seconds after the sliding door was raised. Second, the total time spent on the rail was recorded. Third, it was determined if the animal remained on the rail during the entire one-minute trial. The last two sets of data are similar in that they both are a measure of the animal's ability to maintain balance.

RESULTS

Stationary Rail Test

There was no significant difference between the 1g and 2g rats in their ability to balance using time spent on rail as a measure. Table I indicates that by the fourth day of testing, both groups spent the entire sixty seconds on the rail. During the first three days of testing the 2g animals tended to fall earlier in the trial, but the group differences are not significant.

When the groups were compared as to whether each rat spent the entire sixty seconds on the rail, significant differences were seen on the first two days of testing (day 1, $X^2 = 82$, $p < .01$; day 2, $X^2 = 12.5$, $p < .01$). On the first two days rats in both groups performed better at maintaining balance on the stationary bar. During these first two days, the 2g group appeared to improve at a greater rate. On the third and subsequent days, there was no significant difference between the two groups.

When avoidance was examined it was found that the two groups differed significantly on all days but the first and fifth days. On all days, including the first and fifth days, the 2g rats avoided the shock more often than the 1 g rats. Both groups improved avoidance scores from the performance on the first day. The 1g group appeared to reach a plateau on the fourth day while the 2g group appeared to reach a plateau on the second day.

Rotating Rail Test

The 1g and 2g rats differed significantly in their performance on the rotating rail. When the time spent on the rail was compared for each group, it was seen that on each of the three days of testing, the 1g group remained on the rail significantly longer (Table IV). When the performance was broken down into categories based on the rate of rotation of the rail, it was found that at faster rates of rail rotation, the differences between the two groups becomes more apparent (Table V). At rail rotation rates of 0 and 5 rpm, summed over the three days of testing, there is no significant difference between the 1g and 2g rats. At 10 rpm, summed over three days, the two groups are significantly different at the 95% level of confidence, while at 15, 20, and 25 rpm rates the groups are significantly different at the 99% level of confidence.

When avoidance was examined, it was found that the two groups differed significantly on all three days of testing (Table VI). The 2g group consistently avoided more frequently than the 1g group.

DISCUSSION

Comparing the differences seen in the 1g and 2g groups, it appears that the rotating rail test is a more sensitive tool in differentiating between the two groups. No significant difference was seen between the two groups in the Stationary Rail Test even though there was a consistent numerical difference when time on rail was used as the discriminative parameter (Table I). Table II, which displays the number of trials when each rat spent the entire time on the rail, revealed a significant difference between the two groups on the first two days. This is reflected in Table V at the 0 and 5 rpm rail rotation speeds, but when the rail speed increased above 5 rpm, the differences between the two groups

14

becomes more apparent. At the higher rail rotation speeds the differences between the two groups appears to be progressively greater as suggested by the increasing "+" values (Table V). This difference may be more significant at rail rotation speeds above 25 rpm.

The 1g and 2g rats differed in their ability to balance. This was consistently obvious to the experimenter, even in the stationary rail test. The 2g rats appeared to have much difficulty in maintaining themselves on the rail. They appeared to "lose their balance" often but soon learned to stay on the rail even though they appeared to have much more difficulty than the 1g animals. These subjective evaluations on my part were not reflected in the scores seen in the Stationary Rail Test. At higher rail rotation speeds in the Rotating Rail Test, however, these differences began to become apparent in the test scores.

The data measuring time on rail, for the first three days in the Stationary Rail Test revealed a consistent, but not significantly different, difference between the 1g and 2g rats (Table I). Similar differences were seen for the first five days when the two groups were compared as to the average number of trials in which each rat spent the entire time on the rail. The data were significantly different for the first two days (Table II). The Rotating Rail Test revealed that the two groups did not differ at 0 and 5 rpm. But when the test became more demanding, i.e., at higher rail rotation speeds, the differences between the two groups became significant.

The data from both tests reveal that both the 1g rats and 2g rats improved their ability to stay on the rail with experience. This is especially apparent when the scores are compared in the Stationary Rail Test which ran for a longer time period. If the "+" values are compared in Table IV, it appears that both groups are improving performance at about the same rate. There is no reason, based on these data, to suggest that the 2g rats will approach the 1g rats in their balancing ability. This raises two questions. First, given enough training (e.g., several weeks) will the 2g rats approach the performance level of the 1g rats? Second, if the 2g rats were to remain in the 1g environment, would they eventually approach the performance of the 1g rats? How long would this take?

It is premature at this time to speculate on the anatomical and/or physiological basis for the behavioral differences seen. The data might suggest that it is a system that is called upon to function more in a dynamic situation (viz., semicircular canals). This may be the case. However, even when balancing on the stationary rail, the 2g rat experiences more difficulty in maintaining balance, implying that other sensory mechanisms may be involved.

The differences seen in avoidance behavior were unexpected. The 2g group avoided consistently more frequently than did the 1g group. Both groups improved their avoidance scores with experience (Table III).

The X^2 values remained high even at the end of ten days of testing, suggesting that the difference between the two groups was remaining constant. The cause for these differences is unknown. We might speculate that the 2g environment has imposed a stress factor that has altered the arousal level in the 2g rats. Possibly the answer may lie with the reported vestibular fibers projecting to the brain stem reticular formation, and the known influence of vestibular stimulation on visceral efferents.

Table 1 - Stationary Rail Test. (1g rats and 2g rats compared as to average time, in seconds, spent on rail during one 60 second trial. Ten rats per group were exposed to ten trials each day for ten days. The groups are not significantly different for any day).

Group	Day									
	1	2	3	4	5	6	7	8	9	10
1g	49.0	52.2	60.0	60.0	60.0	60.0	60.0	60.0	60.0	60.0
2g	38.0	47.3	56.3	60.0	60.0	60.0	60.0	60.0	60.0	60.0
t value	1.46	0.62	4.68							

Table 2 - Stationary Rail Test. (1g rats and 2g rats compared as to average number of trials in which each rat spent entire time on rail. Ten rats per group were exposed to ten trials each day for ten days).

Group	Day									
	1	2	3	4	5	6	7	8	9	10
1g	8.2	9.0	9.6	10.0	10.0	10.0	10.0	10.0	10.0	10.0
2g	1.8	7.0	9.8	9.8	9.8	10.0	10.0	10.0	10.0	10.0
X^2	82.0**	12.5**	0.57							

Table 3- Stationary Rail Test. (1g rats and 2g rats compared as to avoidance responses made each day. Ten rats per group were exposed to ten trials per day for ten days).

Group	Day									
	1	2	3	4	5	6	7	8	9	10
1g	.2	.2	.6	3.4	1.8	2.2	2.6	1.6	2.4	2.8
2g	.6	3.6	4.8	5.2	2.8	4.6	5.4	4.6	4.4	5.0
X^2	2.1**	37.4**	44.8**	6.6*	2.8	12.8**	16.1**	21.2**	8.8**	10.2**

Table 4 - Rotating Rail Test. (1g rats and 2g rats compared as to average time, in seconds, spent on rail during one 60 second trial. Ten rats per group were exposed to ten trials each day for three days. Data are averaged for rail speed from zero to 25 rpm).

Group	Day		
	1	2	3
1g	45.2	48.6	52.7
2g	30.5	36.5	35.6
t value	3.49*	3.75*	3.38*

Table 5 - Rotating Rail Test. (1g rats and 2g rats compared as to average time, in seconds, spent on rail during one 60 second trial. Ten rats per group were exposed to ten trials each day for three days. Data are averaged for three days).

Group	Rail Speed (rpm)					
	0	5	10	15	20	25
1g	58.0	54.1	50.9	48.9	40.9	39.2
2g	57.1	47.8	35.1	29.9	22.3	19.8
t value	0.31	1.33	2.48**	3.52*	3.03*	3.62*

Table 6 - Rotating Rail Test. (1g and 2g rats compared as to average number of avoidance responses made each day. Ten rats per group were exposed to ten trials per day for three days).

Group	Day		
	1	2	3
1g	2.2	2.0	2.8
2g	5.0	3.5	3.2
X^2	27.24*	7.56*	6.54*

* significantly different at the 0.05 level (This reference applies to
** significantly different at the 0.01 level (Tables II through VI.

PART III

INTRODUCTION

PHYSIOLOGICAL REVIEW AND MATHEMATICAL BASIS

1. Vestibular Apparatus

The membranous labyrinth is located in the inner ear. It con-
sists of the cochlear duct, three semicircular canals, and two relatively
large sacs known as the utricle and the saccule. The cochlear duct is
concerned with hearing and has nothing to do with equilibrium; the role
of saccule in orientation and postural control is not clearly understood
in higher animals. However, the utricle and the semicircular canals are
important for maintaining equilibrium.

a. Utricle--The macula is the sensory epithelium of the
utricle and consists of sensory cells, a gelatinous substance and many
small calcium carbonate crystals called otoliths. The otoliths are more
dense than the surrounding structures and fluid and, thus, are differ-
entially attracted by gravity. The otoliths are embedded in the upper
surface of the gelatinous substance; below the gelatinous substance are
located many sensory hair cells. Two types of sensory cells have been
identified and are referred to as Type I and Type II. Small sensory
cilia project from the sensory cells into the gelatinous substance.
It is presumed that a shifting of the otoliths results in a shearing
action imparted to the cilia of the sensory cells which action results
in depolarization of the sensory cell.

b. Semicircular Canals--The three semicircular canals, known
as the anterior, posterior, and horizontal (or lateral) semicircular
canals, are arranged at approximately right angles to each other, so
that they roughly form an orthogonal system. The lateral canals lie
in a plane tilted approximately 30 degrees above the horizontal. The
two vertical canals lie approximately vertical to the plane of the
horizontal canal and 90 degrees to each other.

Each canal is in communication with the cavity of the utricle.
At one end of each canal the duct dilates into an enlarged cavity, the
ampulla. The neurosensory epithelium of each semicircular canal lies
within the ampulla.

The neurosensory structure in the ampulla is called the crista
ampullaris. The crista is composed of an overlying gelatinous cupula
and sensory hair cells below. The cupula occludes the ampulla. Cilia
project from the sensory hair cells into the cupula. The cilia in each
crista ampullaris are uniformly directionally oriented.

When the head is rotated in any direction, the endolymph in the semicircular canals tends to remain stationary due to inertia. The inertia force causes deflection of the cupula. Deflection of the cupula results in a shearing force transmitted to the cilia of the sensory cells. This action results in depolarization or hyperpolarization of the cell, depending upon the direction of cupular deflection. The appropriate neural signals are transmitted via the eighth cranial nerve to the brainstem, cause a sensation of rotation and induce the compensatory eye movement called nystagmus.

c. Nystagmus--Nystagmus is the reflex eye movement due to a deflection of the cupula. When the head is accelerated about an axis projected vertically through the center of the head, the eyes move slowly in a direction opposite to the direction of rotation with a velocity equal to that with which the head is turning. This is the slow phase of nystagmus. This movement tends to fixate a visual image on the retina, and minimize the displacement of the image on the retina. The rapid return of the eye to a new starting point in the orbit is called the fast phase of nystagmus.

2. System Analysis

In the field of control systems analysis, one of the most important things is to identify the transfer-function of the system, which gives information about the functional organization of the mechanism. From the point of view of system analysis, we are dealing with a very complicated system which has probably a number of feedback loops in the central nervous system and cross-couples with other systems (i.e., otoliths) through the C.N.S. But, on a biological basis it is not possible to determine the open-loop transfer functions in great detail. We can develop an over-all model of the system which explains behavioral "input-output" data and is consistent with known physiological structures.

a. System Transfer Function--The simplified horizontal vestibulo-ocular reflex arc is shown in Fig. 1(a). For convenience in analysis, the system can be grouped and arranged in several block diagrams which is summarized in Fig. 1 (b). This system has multivariable inputs and a single output, but for easy manipulation we have to restrict attention to one input and one output which is shown in Fig. 1 (c). The relation between input and output is expressed by the transfer H(s) in the complex frequency domain:

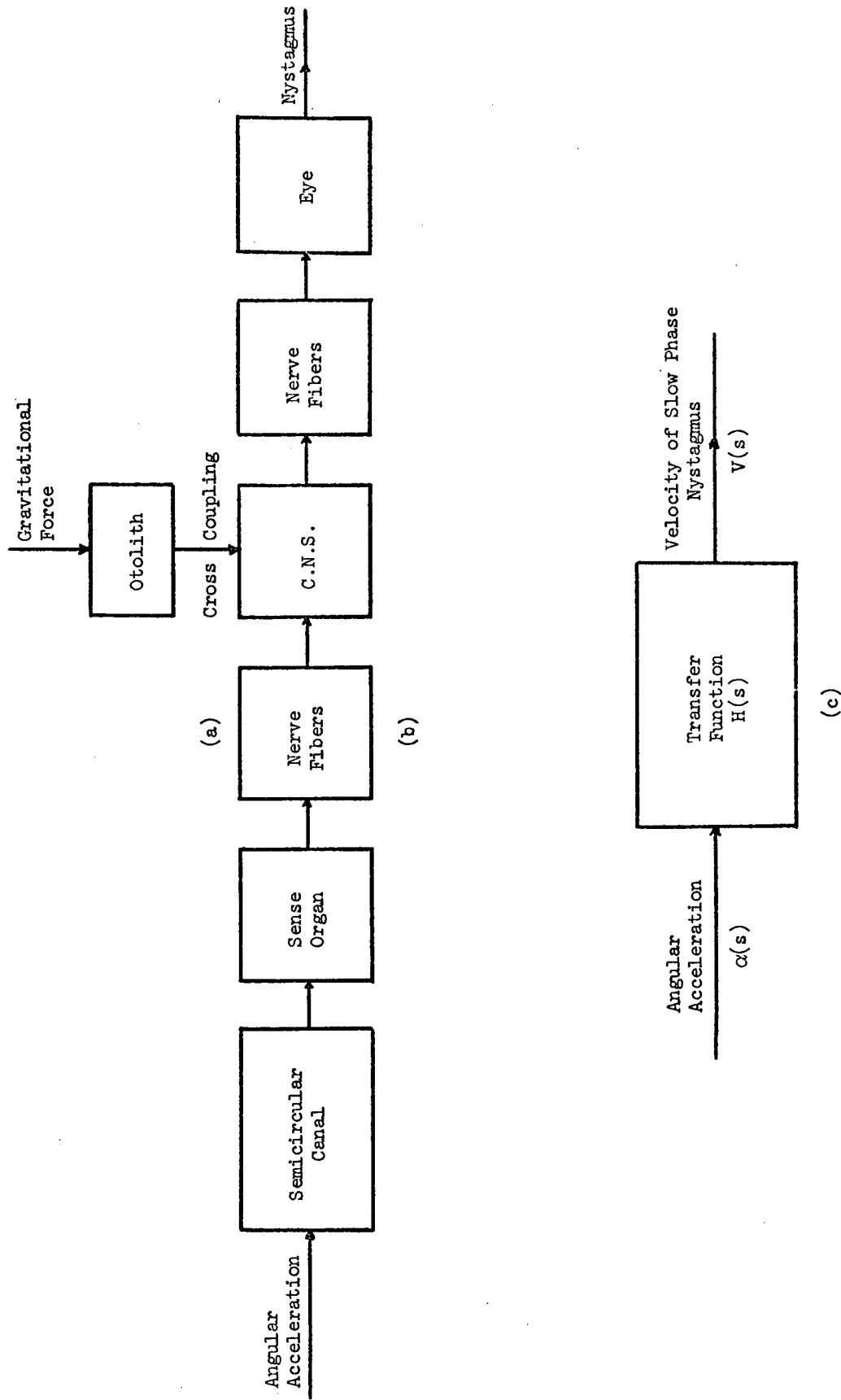$$H(s) = \frac{V(s)}{\Phi(s)} \tag{1}$$

(a)

(b)

(c)

Fig. 1 (a) The simplified horizontal vestibulo-ocular reflex arc in block diagram.
(b) The arrows indicate the direction of information flow.
(c) The simplified transfer function with input [α(s)] and output [V(s)].

21

where

$\ddot{\Phi}(s)$ = Laplace transform of the input angular acceleration, and

$V(s)$ = Laplace transform of the velocity of slow-phase nystagmus.

Since the time function of the velocity of slow-phase nystagmus following an impulse input has the form of an exponential decay, the system transfer function $H(s)$ can be assumed to be:

$$H(s) = \frac{b_{n-1}s^{n-1} + b_{n-2}s^{n-2} + \ldots + b_2 s^2 + b_1 s + b_0}{(s + 1/a_1)(s + 1/a_2)\ldots\ldots(s + 1/a_n)} \qquad (2)$$

where a_1, a_2, $\cdots$, a_n, b_0, b_1, b_2, $\cdots$, b_{n-2}, b_{n-1} are constants to be determined. Taking the partial fraction expansion of Eq. (2) gives

$$H(s) = \frac{A_1}{s + 1/a_1} + \frac{A_2}{s + 1/a_2} + \ldots + \frac{A_n}{s + 1/a_n} \qquad (3)$$

Then, let the input be an impulse function

$$\ddot{\varphi}(t) = \gamma\delta(t) \qquad (4)$$

where $\delta(t)$ is the unit impulse function and γ is the magnitude of the impulse. The corresponding Laplace transform function of $\ddot{\varphi}(t)$ is

$$\ddot{\Phi}(s) = \gamma. \qquad (5)$$

Substituting Eqs. (3) and (5) into Eq. (1), then

$$V(s) = \ddot{\Phi}(s)H(s)$$

$$= \gamma\left(\frac{A_1}{s + 1/a_1} + \frac{A_2}{s + 1/a_2} + \ldots + \frac{A_n}{s + 1/a_n}\right). \qquad (6)$$

The impulse response function is

$$v(t) = \gamma\left(A_1 e^{-t/a_1} + A_2 e^{-t/a_2} + \ldots + A_n e^{-t/a_n}\right) \qquad (7)$$

22

The impulse stimulus gives rise to an after-discharge of nystagmus called post-rotatory nystagmus which is the impulse response. The actual electrical recording of the ocular nystagmus is shown in Fig. 2 (a) which indicates the position of the eye. Figure 2 (b) gives the differentiation of the trace. The upper part of (a) shows the slow-phase velocity which follows an exponential decay with respect to time. The slow-phase velocity does not decay to zero, it ceases at certain threshold level v_{min}. The time between the onset of input stimulus and the cessation of nystagmus is called post-rotatory nystagmus.

$$v_{min} = \gamma \left(A_1 e^{-T_p/a_1} + A_2 e^{-T_p/a_2} + \ldots + A_n e^{-T_p/a_n} \right)$$

$$\frac{1}{\gamma} = \frac{A_1}{v_{min}} e^{-T_p/a_1} + \frac{A_2}{v_{min}} e^{-T_p/a_2} + \ldots + \frac{A_n}{v_{min}} e^{-T_p/a_n} \qquad (8)$$

where

T_p = duration of post-rotatory nystagmus, and

v_{min} = the minimum slow-phase eye velocity at the end of nystagmus.

If the values of γ are varied and then the values of $1/\gamma$ are plotted in logarithmic scale vs. each corresponding T_p, the time constant of each exponent can be extracted from the curve, provided they are adequately separated. Practically, the input stimulations are pulses. It is shown (see Appendix) that the same time constants occur whether or not the input is an impulse or a pulse of finite width.

b. Dynamic Characteristics of the Semicircular Canals

(i) Transfer function of the canal--Although overall transfer function discovery is very important in system analysis, identifying each single physical component of the system would give more details about the system dynamics. Fortunately, based on its physical structures and characteristics, the mechanics of the semi-circular canal can be described by a simple second-order differential equation.

As early as 1931, Steinhausen pointed out that the moment of inertia of the endolymph, the stiffness of the cupula and the viscous friction of the fluid in the canal provide this system with the proper-ties of a heavily damped torsion pendulum. In the idealized perfectly circular form of a canal (Fig. 3), the fluid ring can be considered to rotate around the center of the canal. Therefore, Newton's second law states the system dynamics as
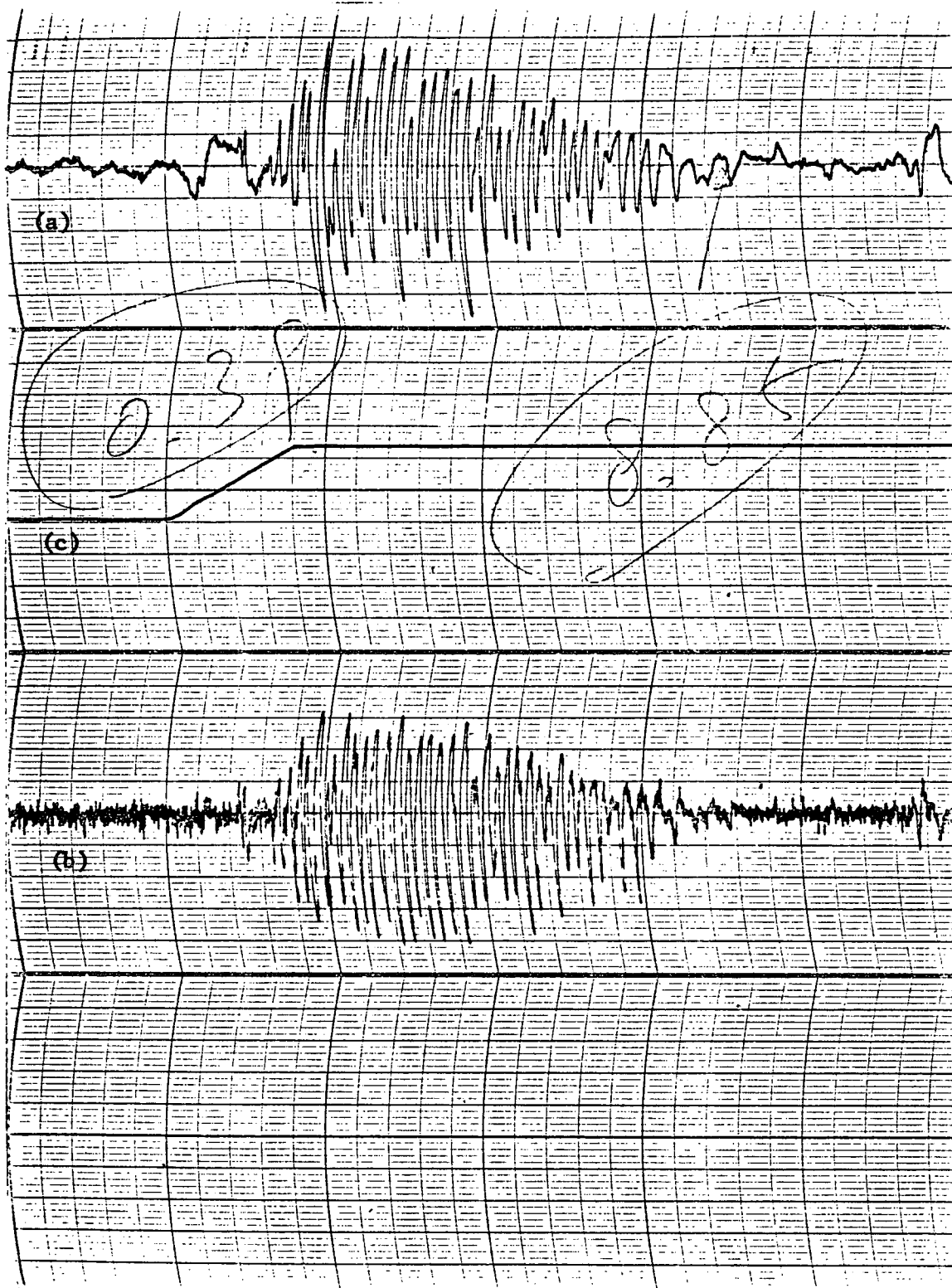
23.

Fig. 2   Recording of post-rotatory ocular nystagmus indicating the
position of the eye (a); the differentiation of the trace (b);
and the inverse of velocity of the turntable (c).

24
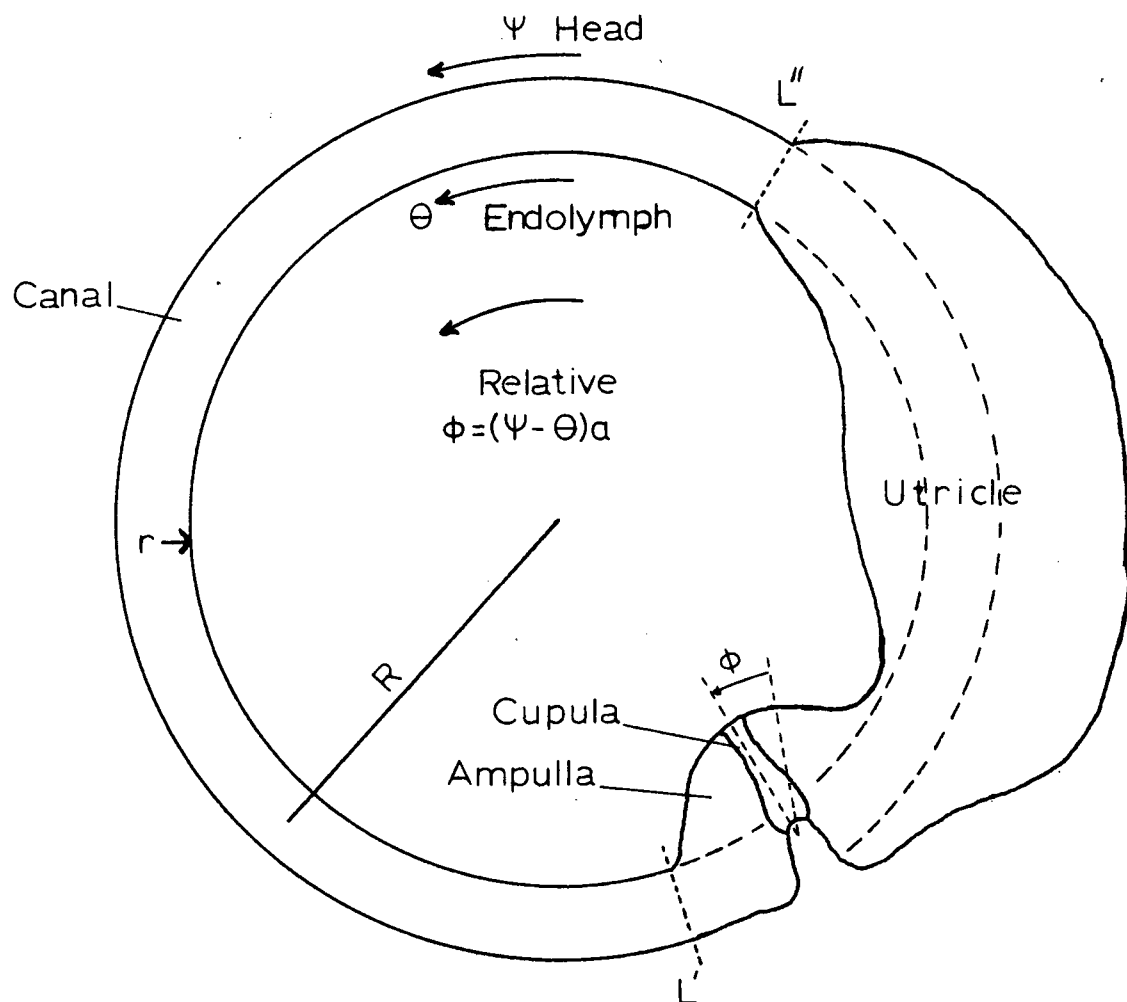
Fig. 3 Idealized form of the horizontal semicircular canal.

$$\Pi(\dot{\phi} - \dot{\psi}) + \Delta(\phi - \psi) = \Theta\ddot{\psi} \tag{9}$$

where

Θ = moment of inertia of the fluid in the canal,

Π = viscous friction at unit angular velocity, and

Δ = stiffness of the cupula at unit angular displacement

Although Eq. (9) provides the correct absolute space relations, we are interested in the relative angular displacement ξ which causes the neural output. Thus, we define k as cupula deflection per unit relative angular displacement between head and fluid, and

$$\xi = k(\phi - \psi) \tag{10}$$

Substituting Eq. (10) into Eq. (9)

$$\Theta\ddot{\xi} + \Pi\dot{\xi} + \Delta\xi = k\Theta\ddot{\phi} \tag{11}$$

This is the linear second-order differential equation for the endolymph-cupula system. The corresponding transfer function of Eq. (11) is

$$\frac{\Xi(s)}{\ddot{\Phi}(s)} = \frac{k}{s^2 + (\Pi/\Theta)s + (\Delta/\Theta)} \tag{12}$$

A second-order equation can be considered as made up of two cascaded first-order lags, i.e.,

$$\frac{\Xi(s)}{\ddot{\Phi}(s)} = \frac{k}{(s + 1/T_1)(s + 1/T_2)} \tag{13}$$

Comparison of Eqs. (12) and (13) yields

$$T_1 T_2 = \Theta/\Delta \qquad T_1 + T_2 = \Pi/\Delta \tag{14}$$

In the case of a highly overdamped system, it turns out $T_1 \gg T_2$. Solving Eq. (14)

26

$$T_1 \approx \Pi/\Delta \qquad T_2 \approx \Theta/\Pi \qquad (15)$$

Substituting Eq. (15) into Eq. (13) gives

$$\frac{\Xi(s)}{\ddot{\Phi}(s)} \approx \frac{k}{(s + \Delta/\Pi)(s + \Pi/\Theta)} \qquad (16)$$

(ii) Impulse response—The constants in Eq. (16) must be determined in order to predict any conduct of the cupula found in practice. One way to solve this problem is to use a series of impulse stimuli with different magnitudes. The constants can be found by analyzing the output response. Substituting Eq. (5) into Eq. (16)

$$\Xi(s) \approx \frac{k\gamma}{(s + \Delta/\Pi)(s + \Pi/\Theta)} \qquad (17)$$

By taking partial fraction of Eq. (17) and using $\Pi/\Theta \gg \Delta/\Pi$ gives

$$\Xi(s) \approx k\gamma \frac{\Theta}{\Pi} \left(\frac{1}{s + \Delta/\Pi} - \frac{1}{s + \Pi/\Theta} \right) \qquad (18)$$

The corresponding response function is

$$\xi(t) = k\gamma \frac{\Theta}{\Pi} \left(e^{-\frac{\Delta}{\Pi}t} - e^{-\frac{\Pi}{\Theta}t} \right) \qquad (19)$$

Eq. (19) can be approximated further

$$\xi(t) \doteq k\gamma \frac{\Theta}{\Pi} \left(e^{-\frac{\Delta}{\Pi}t} \right) \qquad (20)$$

which points to a strictly exponential decay of ξ with time. It is believed that cupula displacement regulates the rate of discharge of the sensory cells and ampullary nerves. In turn, the neural firing rate is known to regulate the magnitude of responses such as nystagmus. Therefore, it is reasonable to use theoretical cupula displacement during semicircular canal stimulation as an approximate predictor of nystagmus. Then, by taking logarithm on both sides of Eq. (20), the nystagmus expires after T_p sec,

$$T_p = \frac{\Pi}{\Delta} \log_e\left(\frac{k\gamma\Theta}{\Pi\xi_{min}}\right) \tag{21}$$

$$= \frac{\Pi}{\Delta} \log_e\gamma + \frac{\Pi}{\Delta} \log_e \frac{k\Theta}{\Pi\xi_{min}} \tag{22}$$

where ξ_{min} denotes the smallest deviation of the cupula giving rise to a just noticeable nystagmus and T_p is called the duration of post-rotatory nystagmus.

The duration T_p can be plotted in a diagram called "cupulogram" which was originally developed by Van Egmond, Groen, and Jongkees. The steepness of the nystagmus cupulogram should give the value of Π/Δ.

(iii) Pulse response--Theoretically, an impulse of acceleration requires instantaneous stopping of the skull. The term "impulse" here means that the braking time should be infinitesmal. This can not be achieved practically even using an electromagnetic brake. But usually a short pulse with duration less than one-tenth of the response time is considered as an "impulse". When the pulse width can not be further reduced to meet the one-tenth requirement, due to the limitations of the instrument, the "impulse" will become impractical. One way to avoid the difficulty in this time constant discovery problem is to let the width of all pulses be the same.

An angular acceleration pulse with duration τ and magnitude α is shown in Fig. 4 (a).

$$\ddot{\varphi}(t) = \alpha[u(t) - u(t - \tau)] \tag{23}$$

where

$$u(t - \tau) = 1 \quad \text{when} \quad (t - \tau) \geq 0$$

$$= 0 \quad \text{when} \quad (t - \tau) < 0$$

By taking Laplace transform of Eq. (23)

$$\ddot{\Phi}(s) = \alpha\left(\frac{1 - e^{-\tau s}}{s}\right) \tag{24}$$

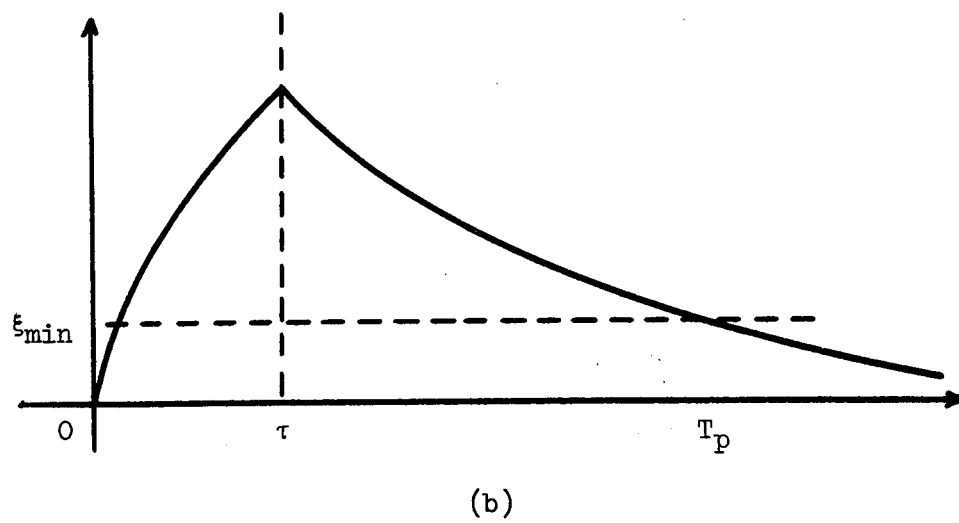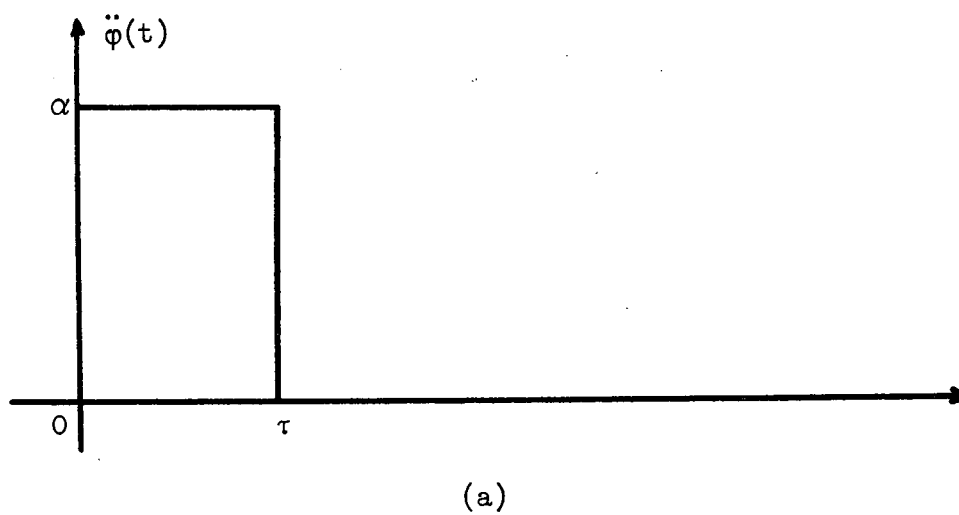Substituting Eq. (24) into (16)

(a)

(b)

Fig. 4 (a) The angular acceleration pulse $\ddot{\varphi}(t) = \alpha[u(t) - u(t - \tau)]$;
(b) the pulse response $\xi(t)$ with ξ_{min} and T_p.

$$\Xi(s) = k\alpha(1 - e^{-\tau s})\left[\frac{1}{s(s + \Delta/\Pi)(s + \Pi/\Theta)}\right] \tag{25}$$

Taking the partial fraction expansion of Eq. (25) and approximating it by $\Pi/\Theta \gg \Delta/\Pi$

$$\Xi(s) = k\alpha\,\frac{\Theta}{\Delta}\left(\frac{1 - e^{-\tau s}}{s} - \frac{1 - e^{\tau s}}{s + \Delta/\Pi}\right) \tag{26}$$

The corresponding pulse response function Fig. 4 (b) is

$$\xi(t) = k\alpha\,\frac{\Theta}{\Delta}\left(1 - e^{-\frac{\Delta}{\Pi}t}\right)u(t)$$
$$- k\alpha\,\frac{\Theta}{\Delta}\left(1 - e^{-\frac{\Delta}{\Pi}(t-\tau)}\right)u(t - \tau) \tag{27}$$

Let $t = T_p$, $\xi(T_p) = \xi_{min}$, and $T_p > \tau$. Equation (27) can be simplified as

$$\xi_{min} = k\alpha\,\frac{\Theta}{\Delta}\,e^{-\frac{\Delta}{\Pi}T_p}\left(e^{\frac{\Delta}{\Pi}\tau} - 1\right) \tag{28}$$

The relation between T_p and α is

$$T_p = \frac{\Pi}{\Delta}\log_e\alpha + \frac{\Pi}{\Delta}\log_e\left(\frac{k\Theta}{\Delta\xi_{min}}\right) + \frac{\Pi}{\Delta}\log_e\left(e^{\frac{\Delta}{\Pi}\tau} - 1\right) \tag{29}$$

This equation, except for $\frac{\Pi}{\Delta}\log_e\left(e^{\frac{\Delta}{\Pi}\tau} - 1\right)$ appearing on the right hand side, is equivalent to Eq. (22). If τ, the width of the pulse, is kept constant, Π/Δ should be given by plotting the cupulogram.

Even the τ's are not the same for all different magnitude pulses, Eq. (29) can still be modified to given the time constant, Π/Δ, through an iteration process. Let

$$C = \frac{\Pi}{\Delta}\log_e\left(e^{\frac{\Delta}{\Pi}\tau} - 1\right) - t \tag{30}$$

30

Equation (29) becomes

$$(T_p - \tau) - C = \frac{\Pi}{\Delta} \log_e \alpha + \frac{\Pi}{\Delta} \log_e \left(\frac{k\Theta}{\Delta \xi_{min}} \right) \tag{31}$$

Thus, a predictor-corrector method which is often used in numerical analysis to solve a differential equation can be similarly applied here to find the value of Π/Δ. Let

$$\text{predictor:} \quad T_p - \tau = \frac{\Pi}{\Delta} \log_e \alpha + \frac{\Pi}{\Delta} \log_e \left(\frac{k\Theta}{\Delta \xi_{min}} \right) \tag{31a}$$

$$\text{corrector:} \quad C = \frac{\Pi}{\Delta} \log_e \left(e^{\frac{\Delta}{\Pi} \tau} - 1 \right) - \tau \tag{30}$$

$$(T_p - \tau) - C = \frac{\Pi}{\Delta} \log_e \alpha + \frac{\Pi}{\Delta} \log_e \left(\frac{k\Theta}{\Delta \xi_{min}} \right) \tag{31}$$

Equation (31a) provides the starting value of Π/Δ by graphical method (cupulogram); we then evaluate a set of C's from Eq. (30) and substitute in Eq. (31) to generate a new value of Π/Δ graphically. Next we evaluate a new set of C's based on the new Π/Δ and again use Eq. (31) to obtain a next Π/Δ. This iteration process is terminated when two successive iterates agree to the desired accuracy.

(iv) Step response--The vestibular model can also be tested by using steps of constant acceleration and observing the latency between the onset of constant angular acceleration and the beginning of the nystagmus, Fig. 2 (b). The latency may be attributed to the fact that a threshold nonlinearity exists in the eye dynamics or in the C.N.S.

The step response can be obtained by letting τ approach infinity in Eq. (27), therefore

$$\xi(t) = k\alpha \frac{\Theta}{\Delta} \left(1 - e^{-\frac{\Delta}{\Pi} t} \right) u(t) \tag{32}$$

since

$$\lim_{\tau \to \infty} u(t - \tau) = 0$$

31

Assume ξ_{th} is the corresponding threshold deviation of the cupula and T_L is the latency of nystagmus,

$$\xi_{th} = k\alpha \frac{\Theta}{\Delta}\left(1 - e^{-\frac{\Delta}{\Pi}T_L}\right) \qquad (33)$$

If α reaches α_{th} which is the constant angular acceleration required to produce a threshold deviation, the latency time, T_L, will approach infinity. Thus,

$$\xi_{th} = k\alpha_{th} \frac{\Theta}{\Delta} \qquad (34)$$

Substitute ξ_{th} in Eq. (33) by

$$\frac{\alpha_{th}}{\alpha} = 1 - e^{-\frac{\Delta}{\Pi}T_L} \qquad (35)$$

The threshold acceleration α_{th} can be given by having Eq. (35) best fit the experimental data, provided Π/Δ is known.

(v) Theoretical value of Θ, Π and Δ--When the anatomical data concerning the semicircular canal are known, the constants of the fundamental differential equation, Eq. (11), of the cupula-endolymph system may be calculated on the basis of fluid dynamics.

The moment of inertia Θ is evaluated on the assumption that the endolymph ring keeps the same cross section even in the utricle. That is, the canal extends itself through the utricle, contributing to the moment of inertia but not to the friction. Then, Θ (from Van Egmond) is expressed as

$$\Theta \doteqdot 2\pi^2\sigma r^2 R^3 \qquad (36)$$

where

σ = density of the endolymph,

r = cross-section radius of the canal, and

R = radius of curvature of the canal.

32

The viscous friction Π is given by

$$\pi = 8\pi\eta R^2 L \qquad (37)$$

where

η = viscosity of endolymph, and

L = length of canal.

The mean canal length of the rat, 1.28 πR, is approximately two-thirds of its circumference. By substituting L = 1.28 πR into Eq. (37)

$$\Pi = 10.24\ \pi^2\eta R^3 \qquad (38)$$

The stiffness of the cupula $\triangle$ is given by

$$\triangle = \pi\mu r^2 R \qquad (39)$$

where μ is the coefficient of elasticity.

Therefore, dividing Π and Θ by $\triangle$ and Π, respectively, gives the value of two time constants Eq. (15)

$$T_1 = \frac{\Pi}{\triangle} = \frac{10.24\ \pi\eta R^2}{\mu r^2} \qquad (40)$$

$$T_2 = \frac{\Theta}{\Pi} = \frac{\sigma r^2}{5.12\ \eta} \qquad (41)$$

RESULTS

TIME CONSTANTS OF THE SYSTEM

The duration of post-rotatory nystagmus for each pulse input is determined. Tables 1 and 2 list the means and standard deviations of duration for 1g and 2g rats, respectively.

33

Table 1   The means and standard deviations of duration
of post-rotatory nystagmus for 1g rats

DECELERATION RATE	DURATION OF POST-ROTATORY NYSTAGMUS (sec)	
(^{o}/sec^2)	MEAN	STANDARD DEVIATION
20	4.03	0.73
25	4.06	0.72
30	3.41	0.53
40	4.34	1.11
50	4.84	1.02
60	4.46	0.97
80	6.16	1.25
100	6.36	2.09
125	7.80	3.51
150	9.04	2.40
200	11.50	3.26
250	14.32	3.37
300	15.12	2.82

Table 2   The means and standard deviations of duration
of post-rotatory nystagmus for 2g rats

DECELERATION RATE	DURATION OF POST-ROTATORY NYSTAGMUS (sec)	
(^{o}/sec^2)	MEAN	STANDARD DEVIATION
50	3.77	0.57
60	3.85	1.09
80	3.92	0.68
100	4.31	0.65
125	5.00	1.07
150	5.04	1.14
200	6.68	1.36
250	8.71	2.06
300	10.09	1.40

The durations as a function of the inverse of deceleration rate are plotted in Fig. 5 (1g) and Fig. 6 (2g), which are essentially the same as cupulograms. The solid curves are chosen to best-fit the data. If the vestibular system could be simply described by a second-order equation (Eq. 11), the cupulogram corresponding to it should reveal a straight line response (Eq. 22). However, since the response in Fig. 5 is considered as a second-order curve by regression analysis, it suggests that the overall response includes more than one exponential term (Eq. 8 and A-9).

A logarithmic ordinate is chosen so that any single exponential decay should be revealed as a straight line. Although the curve in Fig. 5 is curved initially, it does eventually tend to a straight line, suggesting that this part of the response can be approximated by the slowest exponential term, because all faster exponentials have decayed to zero by this time. The slope of this straight portion gives the corresponding time constant. The straight part is then subtracted from the over-all response curve. The new curve is superimposed on Fig. 5. Again, as T_p increases, a single exponential is present with a shorter time constant. After a further repetition, a straight line is obtained, so that the process ends. The same technique is then applied in Fig. 6. Table 3 summarizes the time constants from the response curves of 1g and 2g rats.

A different set of deceleration rates with varying pulse widths were used to test 1g rats. The corresponding results are summarized in Table 4. A method called the predictor-corrector method, which is described by Eqs. (30), (31), and (31a), can be applied to evaluate the Π value of Π/Δ. Figure 7 shows the procedures of the method and indicates the resulting Π/Δ (9.1 sec., approximately).

Using Eq. (41), $\Theta/\Pi = \alpha r^2/5.12\,\eta$, with $\alpha = 1.0087$ g/cm^3, $\eta = 0.0115$ g/cm and $\gamma = 0.0091$ cm, gives us another time constant, $T_2 = 1.42 \times 10^{-3}$ sec, of the semicircular canal. Since this value is too small, none of the suggested methods which were described previously can reveal it. The time constants of the semicircular canal can be summarized as $T_1 = \Pi/\Delta = 9.1$ sec and $T_2 = \Theta/\Pi = 1.42 \times 10^{-3}$ sec.

INPUT THRESHOLD LEVEL OF THE SYSTEM

The mean latency of nystagmus corresponding to each input deceleration is listed in Tables 5 and 6 for 1g and 2g rats, respectively.

The latencies, as a function of deceleration, are shown in Figs. 8 and 9. By using Eq. (35) with known $\Pi/\Delta = 9.05$ for 1g rats and $\Pi/\Delta = 8.42$ for the 2g rats, the value can be adjusted until the equation fits the experimental data. The solid curve in Fig. 8 gives $\alpha t = 5°/\text{sec}^2$ for 1G rats and the one in Fig. 9 shows a higher input threshold level ($11°/\text{sec}^2$) for the 2g rats.
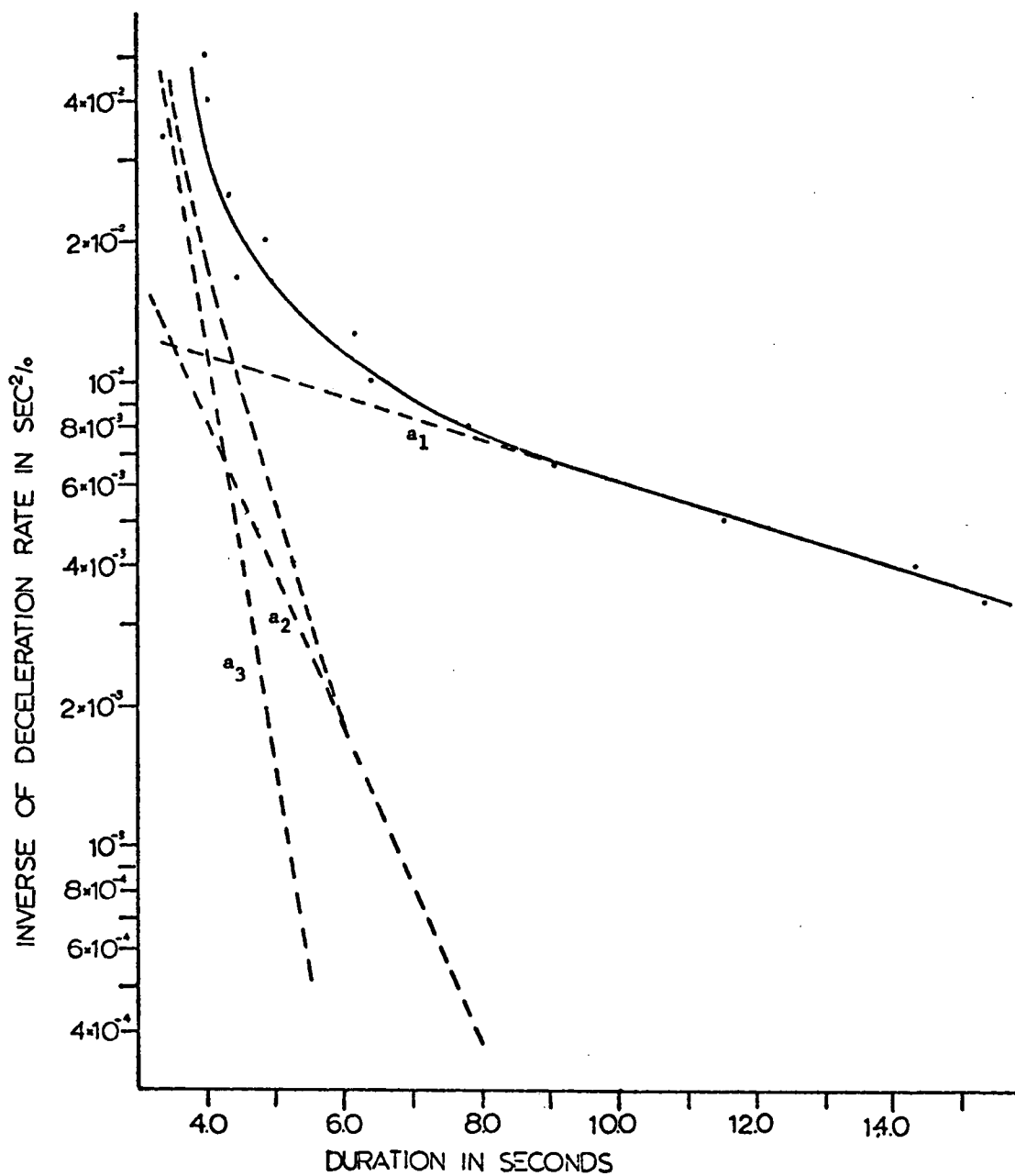
Fig. 5 Mean duration as a function of inverse deceleration
rate for six lg rats. The slopes of the three straight
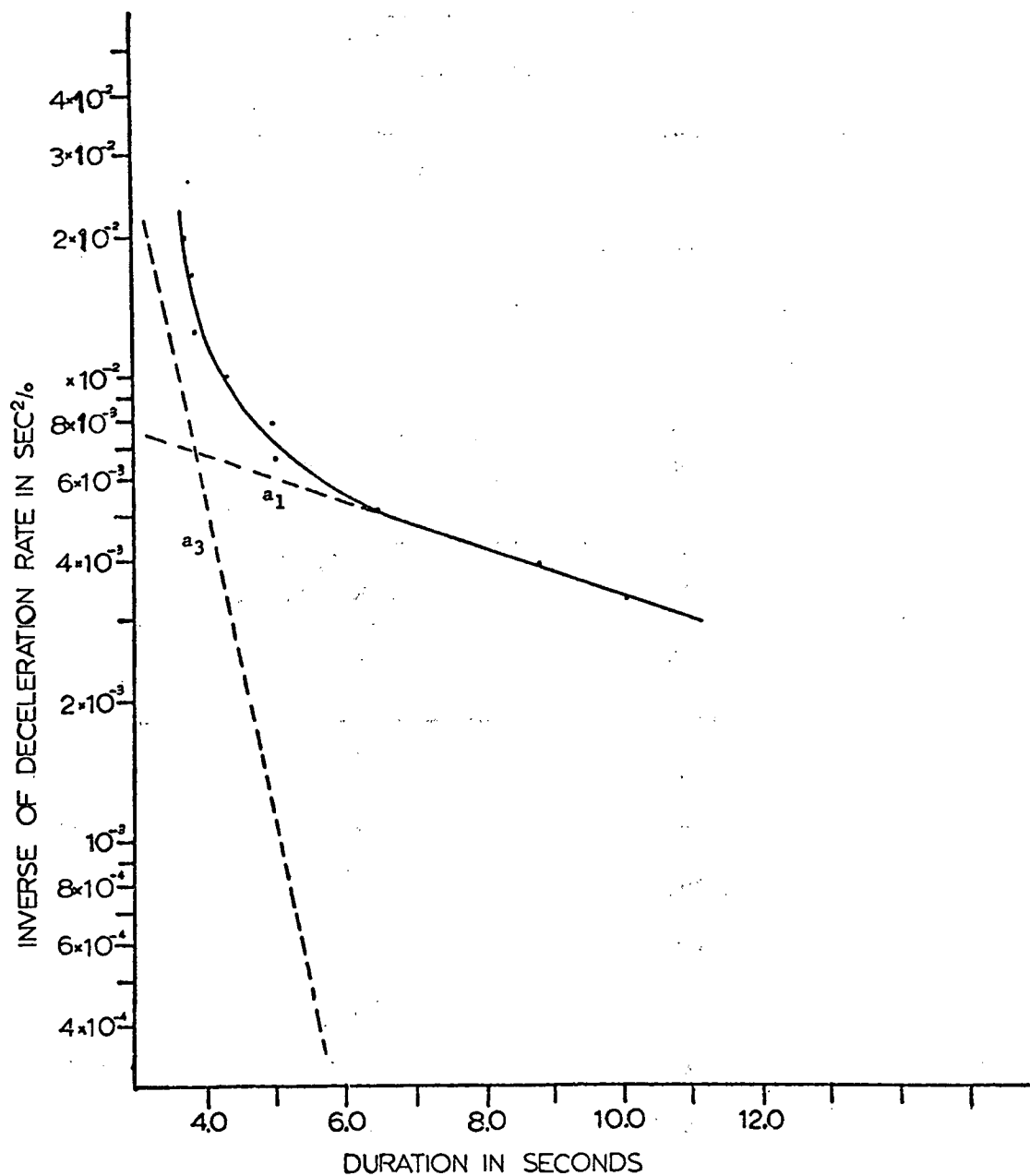lines give the time constants of the system: 9.05,
1.30, and 0.39.

Fig. 6 Mean duration as a function of inverse deceleration rate
for eight 2g rats. The missing time constant of 1.30
shows the difference between 1g and 2g rats.

Table 3   The time constants of 1g and 2g rats

	TIME CONSTANT (sec)		
	a_1	a_2	a_3
1G	9.05	1.30	0.39
2G	8.41		0.30

Table 4   Mean duration of post-rotatory
nystagmus (T_p) for 1g rats

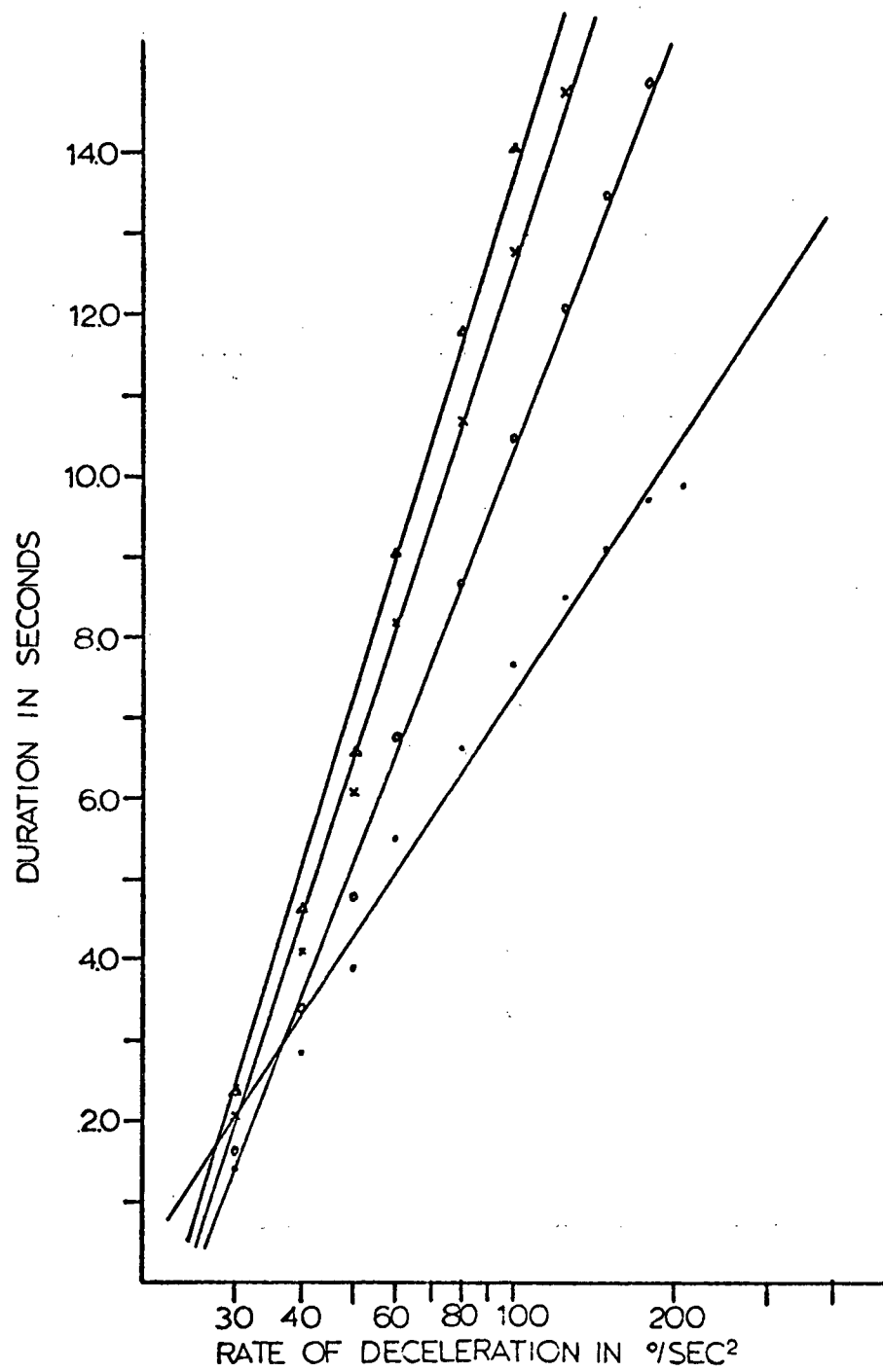| DECELERATION RATE	DECELERATION TIME	MEAN DURATION OF POST-ROTATORY NYSTAGMUS	
($^\circ$/sec^2)	(sec) τ	(sec) T_p	$T_p - \tau$
30	20.0	21.43	1.43
40	15.0	17.78	2.78
50	12.0	15.91	3.91
60	10.0	15.50	5.50
80	7.5	14.09	6.59
100	6.0	13.71	7.71
125	4.8	13.09	8.29
150	4.0	13.05	9.05
180	3.33	13.01	9.68
210	2.86	12.67	9.81

Fig. 7 A predictor-corrector method indicates the
value of Π/Δ, 9.1, approximately.

Table 5   The mean and standard deviation of latency
of nystagmus for 1g rats

DECELERATION RATE	LATENCY OF NYSTAGMUS (sec)	
(^{o}/sec^2)	MEAN	STANDARD DEVIATION
20	2.96	2.16
25	1.20	0.35
30	1.39	0.64
40	1.00	0.43
50	0.75	0.14
60	0.77	0.33
80	0.63	0.25
100	0.56	0.21
125	0.40	0.09
150	0.37	0.11
200	0.27	0.06
250	0.25	0.06
300	0.21	0.08

Table 6 The mean and standard deviation of latency
of nystagmus for 2g rats

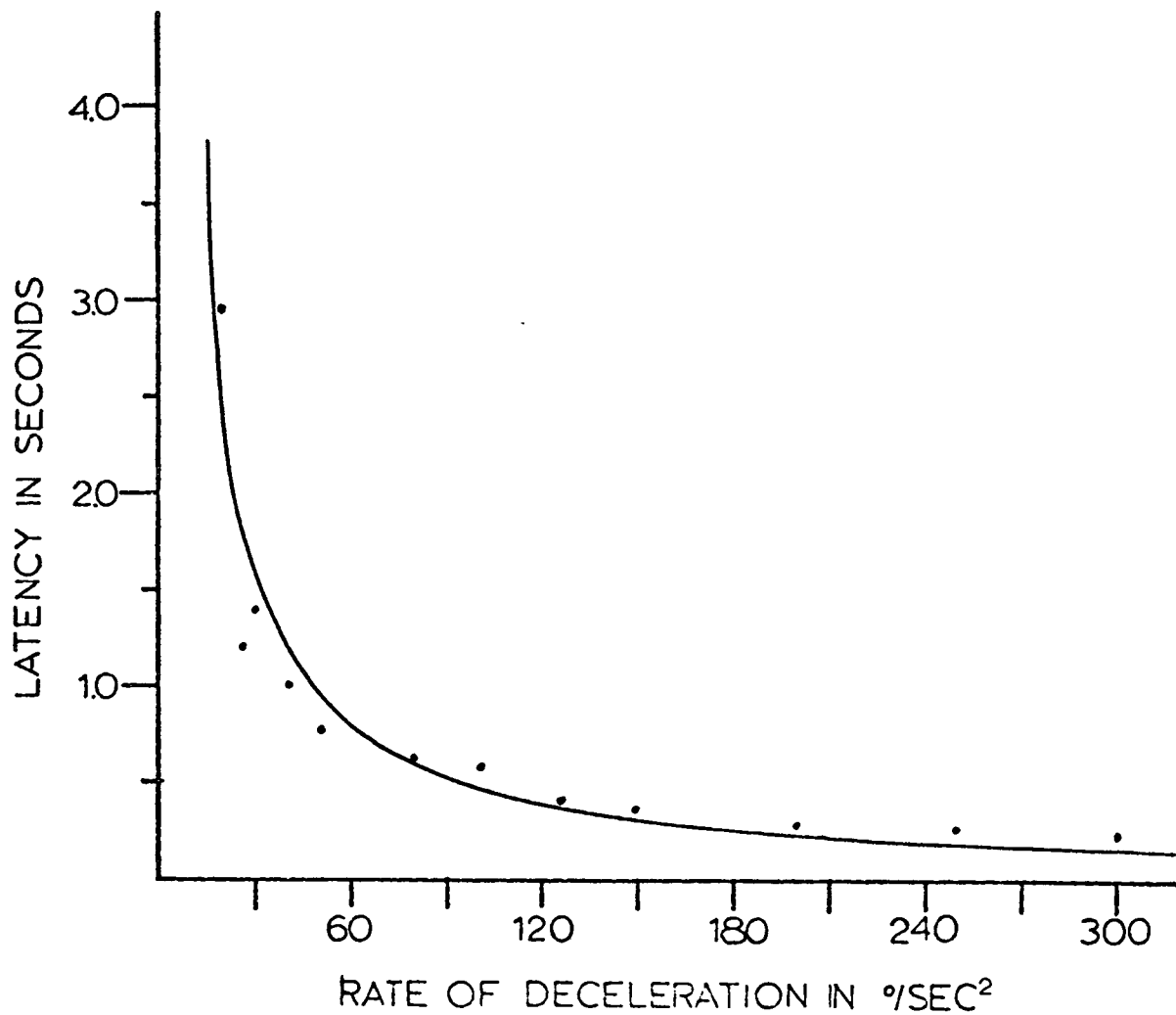| DECELERATION RATE	LATENCY OF NYSTAGMUS (sec)	
(^{o}/sec^2)	MEAN	STANDARD DEVIATION
20	12.82	5.93
30	2.90	1.36
40	2.72	1.58
50	1.35	0.17
60	1.64	0.62
80	1.20	0.50
100	0.98	0.38
125	0.95	0.36
150	0.80	0.31
200	0.56	0.16
250	0.41	0.17
300	0.39	0.15

Fig. 8 The latency of nystagmus following the onset
of constant angular deceleration for 1g rats.
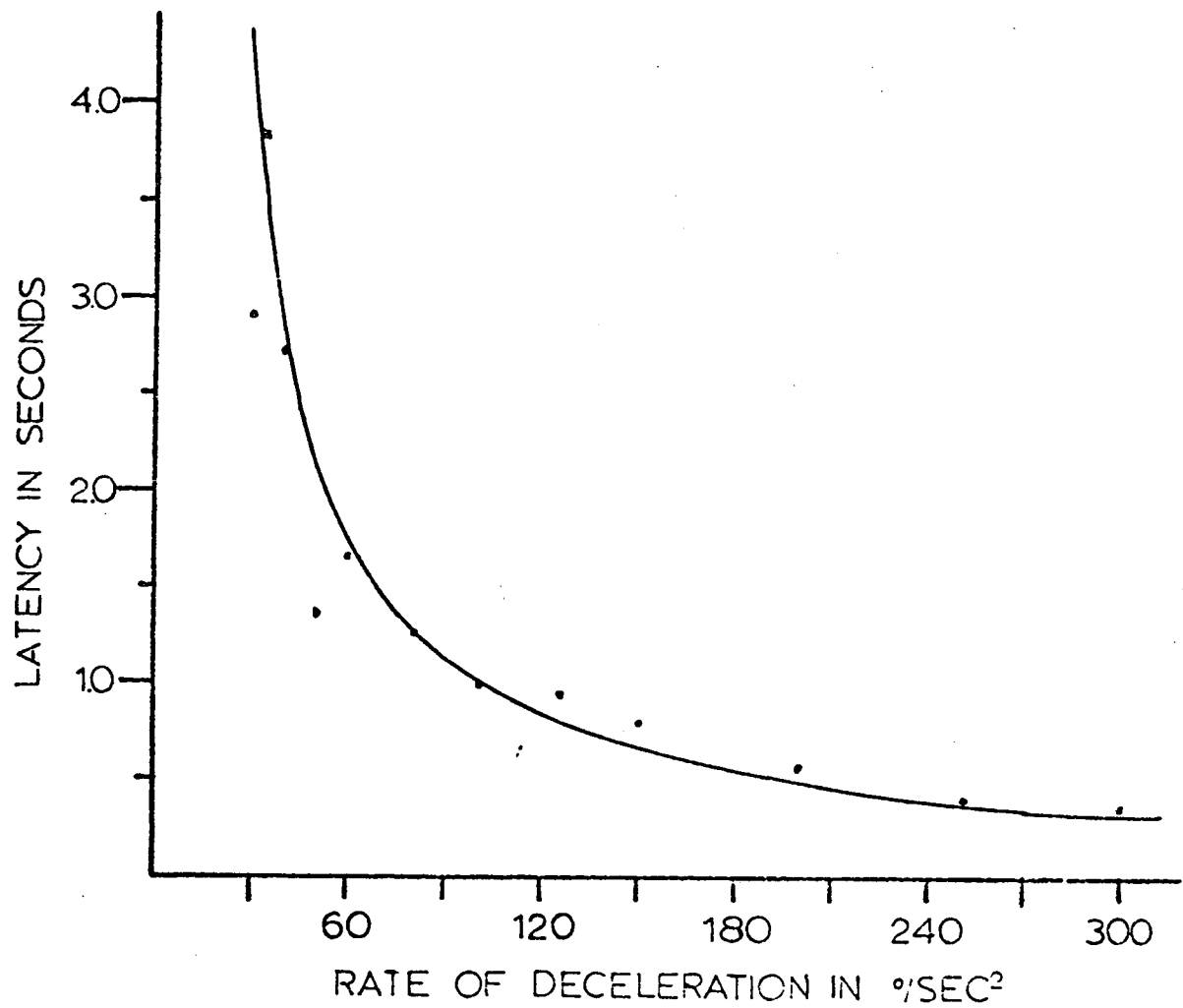The threshold deceleration is $5°/sec^2$.

Fig. 9 The latency of nystagmus for 2g rats. The
threshold deceleration indicates a higher
threshold level of $11°/sec^2$.

DISCUSSION AND CONCLUSION

One of the primary purposes of this study is to evaluate pulse wave forms of angular decelerations and the response they elicit as a means of discovering the time constants of system in vestibular nystagmus response. Pulse waveforms were selected as a test stimuli because they eliminated the difficulties due to the limitations of the stimulator and provided an adequate method to test the rats.

However, the main goal is to find the response difference between rats chronically exposed to a 1g and 2g environment on a basis of biocybernetic models of the horizontal vestibulo-ocular reflex arc. Before presenting the models, the time constants in Table 3 should first be related to the physical model.

Deceleration rates with varying pulse width were selected as stimuli. The advantage of using longer widths for low deceleration rates (Table 4) is to minimize the effect of exponential terms with shorter time constants on the overall response. Therefore, the system tends to respond as a first-order system under these special stimulations. Although the cupulogram (Fig. 7) showed a straight line response, corrections are still needed to evaluate the actual value of Π/Δ.

The value of Π/Δ, 9.1 sec, is close to both a_1's. We can assume a_1 is attributed by the semicircular canal. Π/Δ is determined by the canal's physical dimensions Eq. (40) which are not changed during chronic centrifugation. Assume the physical properties of canal, μ, η and σ, are not changed. The value of Π/Δ in either state should be equal to each other. Again the values of a_1 shows the validity of this assumption.

Comparing the time constants in Table 4 with the block diagrams in Fig. 6 (a) leads to two assumptions. First, a_3 may be related to eye dynamics which is not affected by the chronic 2g state. Ten Kate suggested a value between 0.25 and 3.97 sec for the time constant of pike's eye dynamics and a value of 0.32 sec for the cat. This may further support the hypothesis.

a_2 may be contributed by the utriculus via the C.N.S. Since linear acceleration influences the responses of the semicircular canals, a prolonged 2g state may interfere in some way with the vestibular response. The resulting effect could be the reason for the missing a_2 in the response of 2g rats.

The forces produced by gravitation, linear acceleration, and centrifugation are identical with respect to their effect on organisms. However, centrifugation differs from the other in that it involves a rotation. The coriolis acceleration produced by body motions in a rotating environment may habituate the nystagmus response and lead to the absence of a_2. This will need to be examined further.

The time constants of the semicircular canal were found as $T_1 = 9.1$ sec and $T_2 = 1.42 \times 10^{-3}$ sec. The inverse of T_1 and T_2 are corresponding to the lower and higher 3-dB frequencies of the canal in frequency domain. Therefore, the bandwidth, i.e., the range of frequency between higher and lower 3-dB frequency, is roughly from 0.11 rad/sec to 705 rad/sec. Mayne stated the bandwidth of the canal appears to cover the range of body movement. Due to the small size and light weight of the rat, its bandwidth should include a range higher than that of a human being (from 0.04 rad/sec to 300 rad/sec).

Summarizing the discussion and the results in the previous section, the mathematical models of 1g and 2g for acceleration input are shown in Fig. 10. The value of 9 is chosen as a nominal value for the semicircular canal. K_1, K_2 and K_3 are gains for each block. The model for canal dynamics follows Eq. (12). The one suggested for eye dynamics describes the damping of the eye muscles, however, T_O is only an assumption. Since the denominator is first order, a first-order term may or may not exist in the numerator.

The threshold which only represents an over-all response of the system is not consistent with any physical structure in the horizontal vestibulo-ocular reflex arc.

Numerous investigators have suggested that the responses of the semicircular canals may be described by a heavily over damped torsion pendulum. This means a nystagmus cupulogram should reveal a straight line response rather than a curve response which was shown in Figs. 6 and 7. It appears that this assumption is too simple and that the deviations from the presupposed mechanical laws point out either other physiological structures may play an important role in vestibular nystagmus response or the semicircular canal itself can not be approximated by a simple linear second-order model. The semicircular canal structure has its nonlinearities in the sense of mechanics. The spring constant of the cupula may not be constant even for small deviations from the resting position; it may be a function of its own position. The damping factor is not linear in its nature and may be in quadratic form or have directional preference.

The difference between the responses of 1g and 2g rats may also be explained by the nonlinear characteristics of the semicircular canals. It is possible that chronic centrifugation may have an effect on the vestibular organs. Anatomical studies on rats exposed to chronic acceleration have shown considerable changes in body size and in tissue composition. These changes may result from the increased apparent density of body tissues and fluids induced by the greater accelerative force. Similarly induced changes in chemical composition of the labyrinth may have resulted from chronic hypergravity. Therefore the density and viscosity of endolymph or the spring coefficient of the cupula may differ from those of 1g rats. These differences, if they exist, could alter the functional characteristics of the semicircular canal.
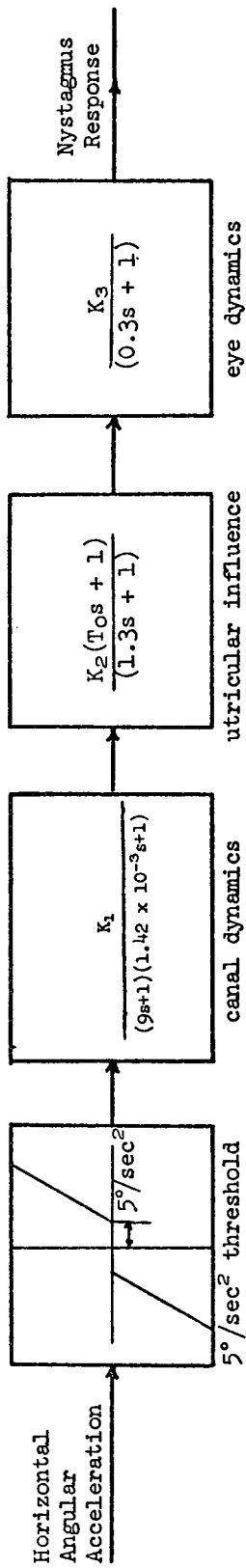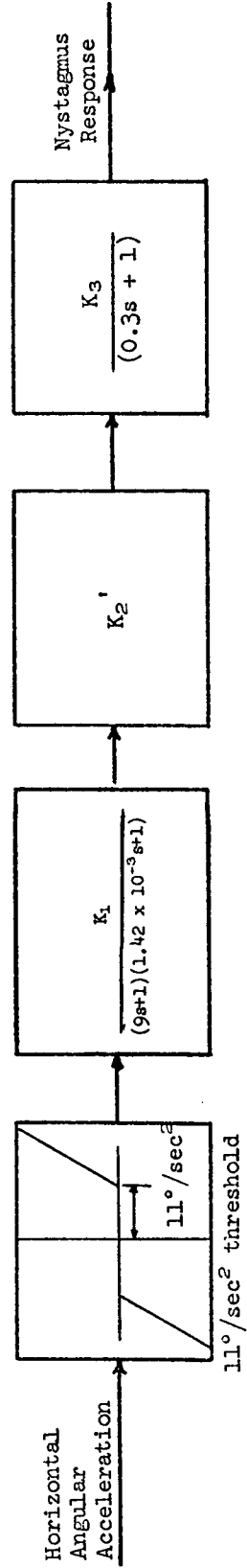
Fig. 10 (a) The mathematical model of 1g for acceleration input. (b) The model of 2g with a missing utricular term and a higher threshold.

46

APPENDIX

An angular acceleration pulse of duration τ and magnitude α can be expressed as

$$\ddot{\varphi}(t) = \alpha[u(t) - u(t - \tau)] \tag{A-1}$$

The corresponding Laplace transform is

$$\ddot{\Phi}(s) = \alpha\left[\frac{1 - e^{-\tau s}}{s}\right] \tag{A-2}$$

Substituting Eq. (A-2) in

$$V(s) = \ddot{\Phi}(s)\left[\frac{b_{n-1}s^{n-1} + \cdots + b_1 s + b_0}{(s + 1/a_1)(s + 1/a_2) \cdots (s + 1/a_n)}\right] \tag{A-3}$$

gives

$$V(s) = \alpha(t - e^{-\tau s})\left[\frac{b_{n-1}s^{n-1} + \cdots + b_1 s + b_0}{s(s + 1/a_1)(s + 1/a_2) \cdots (s + 1/a_n)}\right] \tag{A-4}$$

Take partial fraction of Eq. (A-4)

$$V(s) = \alpha(1 - e^{\tau s})\left(\frac{A_0'}{s} + \frac{A_1'}{s + 1/a_1} + \frac{A_2'}{s + 1/a_2} + \cdots + \frac{A_n'}{s + 1/a_n}\right) \tag{A-5}$$

The corresponding impulse response function is

$$v(t) = \alpha A_0'[u(t) - u(t - \tau)] + \alpha A_1'\left[e^{-t/a_1}u(t) - e^{-(t-\tau)/a_1}u(t - \tau)\right]$$

$$+ \alpha A_2'\left[e^{t/a_2}u(t) - e^{-(t-\tau)/a_2}u(t - \tau)\right] + \cdots$$

$$+ \alpha A_n'\left[e^{-t/a_n}u(t) - e^{-(t-\tau)/a_n}u(t - \tau)\right] \tag{A-6}$$

47

Let T_p be the duration of post-rotatory nystagmus and v_{min} be the minimum slow-phase eye velocity. Then substitute T_p and v_{min} in Eq. (A-6)

$$v_{min} = \alpha A_0' \left[u(T_p) - u(T_p - \tau)\right] + \alpha A_1' \left[e^{-T_p/a_1} u(T_p) - e^{-(T_p-\tau)/a_1} u(T_p - \tau)\right]$$

$$+ \alpha A_2 \left[e^{-T_p/a_1} u(T_p) - e^{-(T_p-\tau)/a_2} u(T_p - \tau)\right]$$

$$+ \cdots A_n' \left[e^{-T_p/a_n} u(T_p) - e^{-(T_p-\tau)/a_n} u(T_p - \tau)\right] \qquad (A-7)$$

Since $T_p > \tau$, Eq. (A-7) becomes

$$v_{min} = \alpha\left[A_1'\left(1 - e^{\tau/a_1}\right)e^{-T_p/a_1} + A_2'\left(1 - e^{\tau/a_2}\right)e^{-T_p/a_2} + \cdots\right.$$

$$\left. + A_n'\left(1 - e^{\tau/a_n}\right)e^{-T_p/a_n}\right] \qquad (A-8)$$

Divide both sides of Eq. (A-8) by

$$\frac{1}{\alpha} = \frac{A_1'}{v_{min}}\left(1 - e^{\tau/a_1}\right)e^{-T_p/a_1} + \frac{A_2'}{v_{min}}\left(1 - e^{\tau/a_2}\right)e^{-T_p/a_2} + \cdots$$

$$+ \frac{A_n'}{v_{min}}\left(1 - e^{\tau/a_n}\right)e^{-T_p/a_n} \qquad (A-9)$$

The relation between α and T_p is equivalent to that of γ and T_p in Eq. (8) except the constant terms $\left(1 - e^{\tau/a_1}\right)$, $\left(1 - e^{\tau/a_2}\right)$, $\cdots$, $\left(1 - e^{\tau/a_n}\right)$ existed in Eq. (A-9). Therefore, the same method can be applied to find the time constants in pulse response.